ISSN 1075-7015, Geology of Ore Deposits, 2015, Vol. 57, No. 6, pp. 465–495. © Pleiades Publishing, Ltd., 2015.
Original Russian Text © G.N. Gamyanin, O.V. Vikent'eva, V.Yu. Prokof'ev, N.S. Bortnikov, 2015, published in Geologiya Rudnykh Mestorozhdenii, 2015, Vol. 57, No. 6, pp. 513–545.

Arkachan: A New Gold–Bismuth–Siderite–Sulfide Type of Deposits in the West Verkhoyansky Tin District, Yakutia

G. N. Gamyanin, O. V. Vikent'eva, V. Yu. Prokof'ev, and N. S. Bortnikov

Institute of Geology of Ore Deposits, Petrography, Mineralogy, and Geochemistry, Russian Academy of Sciences, Staromonetnyi per. 35, Moscow, 119017 Russia

Received June 9, 2014

Abstract—The formation sequence of orebodies, chemical composition of gangue and ore minerals, fluid inclusions, REE patterns, $^{40}Ar/^{39}Ar$ isotopic age, and relationships of stable isotopes (C, O, S) in minerals of the Arkachan gold–bismuth–siderite–sulfide deposit have been studied. The deposit has been localized in the Kuranakh Anticlinorium of the Verkhoyansky Fold–Nappe Belt at the intersection of the near-meridional Kygyltas and the NE-trending North Tirekhtyakh faults. The orebodies are extended (>2 km) and steeply dipping zones of veins and veinlets are hosted in Carbonaceous and Permian sandstones and siltstones deformed in anticlines and cut through by dikes pertaining to diorite–granodiorite–granite association. The deposit was formed during hydrothermal-metamorphic, productive main gold, silver–polymetallic, and silver–antimony stages. The orebodies are largely composed of quartz and siderite; arsenopyrite, pyrite, and pyrrhotite are widespread; bismuthinite, chalcopyrite, sphalerite, galena, and bismuth sulfosalts (gustavite, cosalite, matildite) are less abundant. The REE patterns of carbonates and quartz are characterized by a negative Eu anomaly. Three types of fluid inclusions (FI) in quartz and carbonates are distinguished: (I) liquid $H_2O + CO_2 \pm CH_4 + NaCl$, (II) gaseous $CO_2 \pm CH_4$, and (III) aqueous salt solutions. The homogenization temperature and salinity of FI I vary from 385 to 280°C and 18.8 to 26.2 wt % NaCl equiv, respectively, whereas in FI III these parameters vary from 261 to 324°C and 3.7 to 9.5 wt % NaCl equiv. The pressure is estimated at 1830 to 1060 bar. The $\delta^{18}O$ of quartz II associated with siderite I, native gold, and sulfosalts changes from +13.6 to 16.3‰(SMOW); $\delta^{18}O$ and $\delta^{13}C$ of siderite I related to gold-ore stage vary from +13.6 to +17.7‰ (SMOW) and from –6.0 to –3.0 (PDB). A wide range of $\delta^{34}S$ from –5.7 to 16.0‰ (CDT) has been obtained for sulfides. The isotopic $^{40}Ar/^{39}Ar$ age of muscovite is 101.9 ± 1.4 Ma. The isotopic compositions of C, O, and S in fluids and their REE patterns suggest that magmatic components are predominant. Metamorphic H_2O, CO_2, and occasionally CH_4 are derived from the apical part of a hidden intrusion, whereas sulfur is delivered from country rocks as a result of heating.

DOI: 10.1134/S1075701515060045

INTRODUCTION

The Arkachan gold–bismuth–siderite–sulfide deposit is located on the eastern slope of the Verkhoyansky Range 230 km to the southwest of Batagai Settlement, Sakha-Yakutia Republic, Russia. The gold mineralization of stringer zones in the area of this deposit was revealed by geological mapping in the 1930s. Afterward, economic Au contents were detected (Aristov et al., 2003), and forecasted Au resources were estimated at ~100 t (Zadorozhny, 2002; Bortnikov et al., 2011). In addition to its economic significance, the interest in this deposit is increased by the fact that this is so far the only known large gold deposit in the West Verkhoyansky metallogenic province, where cassiterite–sulfide and silver–base-metal deposits hosted in terrigenous rocks and paragenetically related to granitoids are predominant (Anikina et al., 2010; Gamyanin et al., 1999; Gamyanin, 2001; Konstantinov et al., 2002). As was assumed, tin and gold deposits are related to different metallogenic belts, because gold deposits are, as a rule, associated with oxidized calc-alkaline and alkaline monzodiorites of an I-type (Sillitoe, 1993; Blevin and Chappel, 1995), whereas tin deposits are linked to reduced and silicic S-type granitoids (Lehmann, 1990) in the classification of Chappel and White (2001). However, a number of large gold deposits are actually related to Sn–W provinces and associated with reduced granitic magmas (Thompson et al., 1999; Lang and Baker, 2001). They have been combined into a special class of reduced intrusion-related gold deposits characterized by low contents of sulfides and the occurrence of Bi, W, As, Mo, Te, and/or Sb precipitated from CO_2-enriched fluids (Hart, 2005). The question arises whether Arkachan is related to this class of deposits. At the early stages of research, it was classified as belonging to the chalcopyrite–pyrite–arsenopyrite (mesothermal ?) type of gold-sulfide mineralization (Ivensen et al., 1975). Kostin (2003) compares Arkachan with Galechnoe and Khospokh gold–rare-metal deposits localized in the Derbeke–Nel'gese

[1] Corresponding author: O.V. Vikent'eva. E-mail: ovikenteva@rambler.ru

Zone. Aristov et al. (2003) referred the Arkachan deposit to the gold–quartz type and compared it with the typical mesothermal (Bortnikov et al., 1998) or orogenic (Goldfarb et al., 2005) Nezhdaninsky deposit. We suggest that Arkachan is related to a hidden granitoid intrusion. The close association of native gold with Bi minerals and participation of carbon dioxide fluid in ore formation allowed us to assume its similarity with intrusion-related gold deposits (Bortnikov et al., 2011). At the same time, widespread siderite and sulfides in ore zones indicate its similarity with the silver–polymetallic deposits of this district.

To understand the formation conditions of this deposit and its relationship to silver–tin systems, we have performed a detailed study of mineralogy, geochemistry, stable isotopes, REE pattern, fluid inclusions, and isotopic age of ore. The data obtained allow us to classify the Arkachan deposit as a specific gold–siderite–bismuth–sulfide type, which does not have analogs in the Russian Northeast and is derivative of Sn-bearing ore–magmatic systems.

GEOLOGY

The Arkachan deposit is situated in the West Verkhoyansky zone of the Yana–Kolyma metallogenic province, i.e., in the Verkhoyansky Fold–Nappe Belt extending along the northeastern margin of the Siberian Platform for 2500 km at a width reaching 500 km. This belt was formed from Late Jurassic (~150 Ma) to Late Cretaceous (~80 Ma) (Parfenov, 1999). The deposit is localized in the axial zone of the Kuranakh Anticlinorium at intersection of the near-meridional Kygyltas and the northeastern North Tirekhtyakh regional faults that control the tin-sulfide and tin–silver–polymetallic occurrences and deposits (Fig. 1).

The Arkachan deposit is composed of Carboniferous and Permian terrigenous rocks (Fig. 2), making up a system of asymmetric folds with steep (∠40°–60°) eastern and low-angle (∠20°–30°) western limbs. The largest Left-Arkachan and Right-Arkachan anticlines, 3.0–3.5 km in width, are traced across the entire ore field in a near-meridional direction (∠330°–350°).

The host terrigenous rocks are related to the Solonchan (C_{2-3}sl) and the Kygyltas (C_3kg_1–P_1kg_2) formations. The Solonchan Formation is represented by sandstones and siltstones with claystone and conglomerate interbeds. The orebodies are hosted in rocks of the Kygyltas Formation, which is subdivided in the lower subformation (C_3kg_1) composed of coarse- and medium-grained sandstones, siltstones with fine-grained sandstone interlayers and the upper subformation (P_1kg_2) represented by a member of intercalating medium- and fine-grained sandstones and siltstones.

Igneous rocks at the deposit are represented by dikes pertaining to diorite–granodiorite–granite association, which are conformable to orebodies (Aristov et al., 2003). It cannot be ruled out that they are derivatives of a hidden granitoid pluton. According to geophysical data, its roof occurs at a depth of 1.5–2.7 km (Gutorovich and Izarov, 1966).

Orebodies are extended (>2 km) and steeply dipping vein–veinlet zones. Their width varies from a few meters to 70–100 m. The thickness of veinlets is commonly limited by 0.1–50 cm and occasionally by 10–50 cm (Fig. 3). The density of veinlets is 2–5 to 8–12 items per meter. Six ore zones are traced at the deposit, and only two of them (zones 3 and 4) are economic. According to the results of channel sampling, the Au content reaches few tens gpt, while chip samples along the veinlets, >2 cm in thickness, yield up to 130 g/t. The veinlets branch and become somewhat thicker with depth. The host rocks near veinlets undergo carbonation, sericitization, and silification.

MINERAL ASSEMBLAGES AND CHEMICAL COMPOSITION OF MINERALS

About 40 minerals are known in orebodies of the Arkachan deposit (Table 1). Quartz (50–60 vol %) and siderite (30–35 vol %) are predominant. Contents of early sulfides (arsenopyrite, pyrite, pyrrhotite) amount to 5–10 vol %. Contents of ankerite reach 5 vol %; 1–2 vol % fall on late sulfides (bismuthinite, chalcopyrite, sphalerite, galena) and sulfosalts (gustavite, cosalite, matildite). The abundance of the latter in veinlets is extremely nonuniform.

Based on texture and structures of mineral aggregates and their chronological relationships in veins and veinlets, as well as on spatial distribution in orebodies, we recognize four stages of mineral formation: early hydrothermal–metamorphic, productive main gold, late silver–polymetallic, and final silver–antimony.

The proposed scheme of mineral formation differs from that elaborated by Aristov et al. (2003), who assume that the deposit was formed in two stages. Thin quartz–feldspar veinlets with biotite and preore chlorite–feldspar–quartz metasomatic aggregate were formed at the first stage, whereas the pyrite–sericite–siderite–quartz metasomatic matrix, gold–arsenopyrite–quartz, siderite–quartz–sulfide, chalcopyrite–quartz–siderite, polymetallic, and gold–bismuthinite assemblages arose at the second stage.

Hydrothermal–Metamorphic Stage

Preore almost sulfide-free quartz–carbonate veins and veinlets are characterized by regional abundance at the deposit and nearby. They bear a background (up to 1 g/t) Au mineralization and are not prospecting guides for gold ore. The interstratal lenticular veins of coarse-grained milky-white *quartz I* up to 40 cm in thickness along with columnar quartz–carbonate veins and veinlets are localized in NE-trending fracture zones.

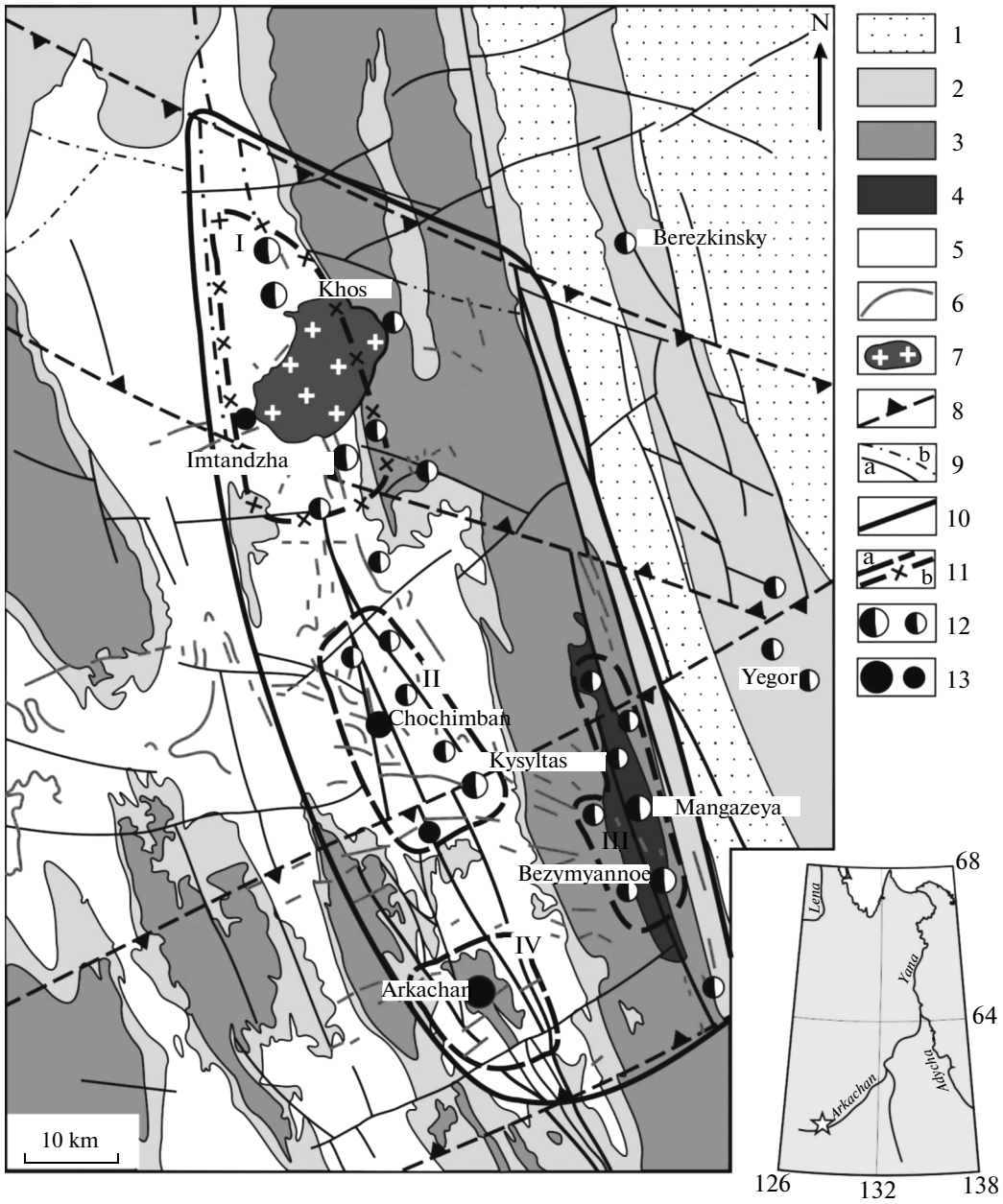

Fig. 1. Geological map of the West Verkhoyansky ore district. (1) Lower Mesozoic sandshale rocks; (2–5) Upper Paleozoic rocks: (2) Permian sandshale rocks, (3) Lower Permian pelitic rocks, (4) Lower Permian conglomerate and sandstone, (5) Carboniferous flyschoid rocks; (6) minor magmatic bodies (Permian–Triassic intermediate sills and Cretaceous felsic dikes and stocks); (7) Early Cretaceous granodioritic and granitic intrusions; (8) zones of tight NW- and NE-trending faults; (9) faults: (a) proved and (b) inferred; (10) contour of ore district; (11) contours of gold (a) and silver–polymetallic (b) ore clusters (I, Khobotu-Echi, II, Nyuetama, III, Mangazeya, IV, Arkachan); (12) silver–polymetallic deposits and occurrences; (13) gold deposits and occurrences.

Ankerite I together quartz I fill veinlets columnar in internal structure and is characterized by elevated SrO content.

Main gold (Productive) Stage

Numerous intersections of quartz–carbonate veins of the early stage by productive quartz–carbonate–sulfide veinlets are noted at the deposit. Mineralogical observations in geological workings and at outcrops display a persistent sequence of mineral formation at the productive stage. The veinlet selvages are overall composed of druses of small transparent quartz crystals, which become larger in bigger voids. Arsenopyrite and pyrrhotite are often observed in heads of large transparent quartz crystals (Fig. 4). Muscovite spher-

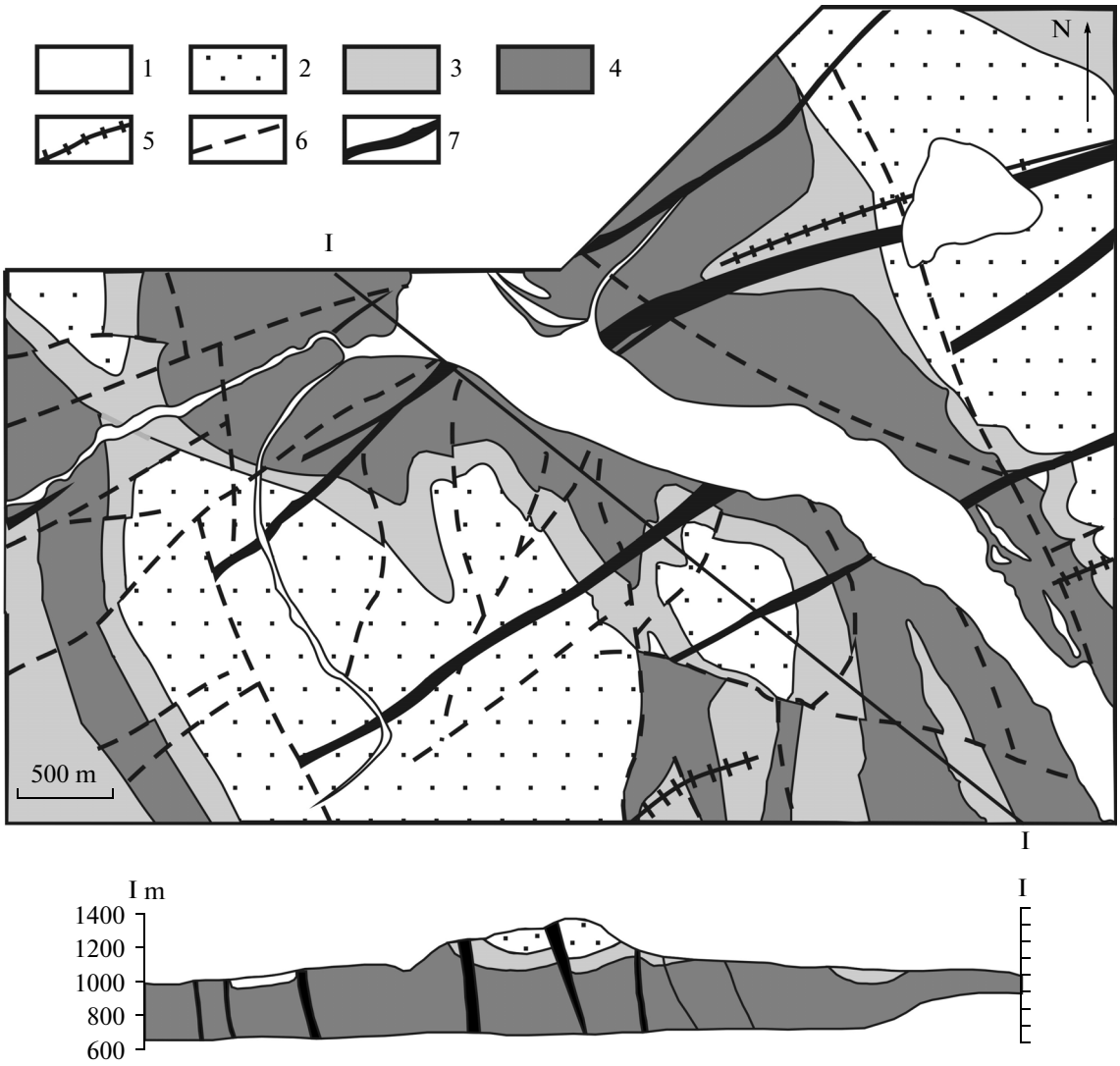

Fig. 2. Geological map and section of Arakchan deposit. (1) Quaternary sediments; (2–4) Upper Carboniferous–Lower Permian Kygyltas Formation (C_3kg_1–P_1kg_2): (2) upper subformation: sandstone, siltstone, sporadic mudstone (P_1kg_2); (3) lower subformation, upper member: siltstone, sandstone with mudstone interbeds ($C_3kg_1^1$); (4) lower subformation, upper member: siltstone and mudstone ($C_3kg_1^2$); (5) granodiorite porphyry dikes, (6) faults; (7) ore zone.

ulites and then arsenopyrite–pyrrhotite aggregates are represented by intergrowths of crystals, as well as massive segregations covering quartz crystals. Siderite precipitated late, frequently as druselike intergrowths. Pyrrhotite is replaced with magnetite–pyrite graphic intergrowths contemporaneously with siderite crystallization. Interstices and microcracks in early sulfides and siderite are filled with chalcopyrite, Bi minerals (bismuthinite, gustavite, cosalite, matildite), and less frequently galena and sphalerite. Native gold is often associated with bismuthinite.

Quartz II is prevalent as the earliest mineral. The specificity of quartz at this deposit consists in its almost constant occurrence as transparent or semitransparent crystals in form of combed selvages.

Siderite I is widespread in ore. Its high MgO contents (microprobe data, see Table 2) allow us to identify this mineral as magnosiderite. The MnO content does not exceed 2% on average. The MgO and Mno contents in siderite distinctly decrease with depth from ore zones 3 and 4. Stringers and disseminations of molybdenite, wolframite, and scheelite occur in quartz II and siderite I.

Pyrite I is rather widespread and reaches 90% of sulfides in particular segments of veins and veinlets. In most cases, pyrite replaces pyrrhotite, although locally it forms coarse-grained aggregates. Pyrite crystals occasionally occur among siderite. According to a microprobe, pyrite I contains 1.0–1.5% arsenic, which is distributed in block fashion. As follows from

the results of emission and atomic-absorption spectroscopy, pyrite I contains Au, Ag, As, Cu, Sb, Ni, Co, Zn, Sn, and Pb (Table 3); Ni, As, Zn, Pb, and Cu contents increase with depth in all orebodies. An inverse tendency is typical of gold, which enriches pyrite at upper levels of zones 3 and 4.

Arsenopyrite I commonly makes up large clusters of perfect or imperfect slightly flattened rhombic crystals (Fig. 4). As a rule, arsenopyrite grows over quartz and is surrounded by siderite I aggregates. Microprobes show that arsenopyrite I contains (wt %): 34.2–34.8 Fe, 41.2–43.9 As, 21.4–22.9 S, as well as 0.05–0.34 Co and up to 0.05 Sb; S/As ratio varies from 1.14 to 1.3 (Table 4). In ore zones 3 and 4, arsenopyrite I is enriched in As with depth. As follows from the results of emission and atomic absorption spectroscopy, arsenopyrite I contains Au, Ag, Cu, Sb, Ni, Co, Bi, Zn, Sn, W, and Pb (Table 3). In contrast to pyrite, arsenopyrite is enriched in Au with depth.

Danaite (arsenopyrite variety containing 6–12 wt % Co) is identified frequently (Table 4). *Glaucodot* (14.4–16.1 wt % Co) has been identified in association with arsenopyrite I. Its chemical composition has been recalculated to the formula $Fe_{0.53–0.58}Co_{0.44–0.45}As_{0.97–0.98}S_{1.01–1.05}$ (Table 4).

Chalcopyrite is a sufficiently abundant mineral, which cements pyrite I and arsenopyrite I aggregates without signs of corrosion or replacement. Chalcopyrite is closely associated with bismuthinite and native gold. Skeletal sphalerite I crystals occur in chalcopyrite at deep levels. According to the results of spectral analysis, chalcopyrite constantly contains (ppm) In (7–50) and Sn (15–700), frequently Ga (10–50), and sporadically Ge (5–10) and Au (3–70).

Sphalerite I is associated with chalcopyrite. Stellate sphalerite I segregations in chalcopyrite and emulsion impregnations of chalcopyrite in sphalerite I at grain margins or close to contact with chalcopyrite are detected at deep levels. Sphalerite I constantly contains 5.1–9.3 wt % Fe (Table 5), up to 2.5 wt % Cu, 0.05–0.48 wt % Cd, and occasionally up to 0.12 wt % Sn, 0.03% In, and 0.25% Mn.

Galena I occurs extremely rarely as stringers in pyrite I and arsenopyrite I or cements their broken aggregates. In some cases separate zones in pyrite I crystals are replaced with galena I (Fig. 4). Rare intergrowths of galena I and sphalerite I with emulsion impregnations of chalcopyrite are noted. The chemical composition of galena is close to stoichiometry (Table 6).

Fahlore I surrounds pyrite aggregates along with chalcopyrite, sphalerite I, galena I and fills interstices in siderite aggregate. The fahlore is represented by tetrahedrite containing (wt %) 25.7–28.1 Sb, up to 0.6 As, and 4.3–6.0 Ag (Table 7). Microprobe results are recalculated to the formula $(Cu_{9.27–9.66}Ag_{0.67–0.94})_{10.08–10.33}(Fe_{0.37–1.47}Zn_{0.49–1.79})_{1.73–2.18}(Sb_{3.60–3.90}As_{0–0.13})_{3.61–3.90}S_{12.94–13.08}$. Stannite and cassiterite were identified in association with chalcopyrite and fahlore I. The formula of stannite $(Cu_{1.99–2.01}Fe_{0.79–0.85}Zn_{0.14–0.15}Sn_{0.98–0.99}S_{4.04–4.06})$ is close to stoichiometry; an isomorphic Zn admixture (~2 wt %) is determined (Table 5). Cassiterite occasionally contains 2.3 wt % W and 1.1 wt % Fe.

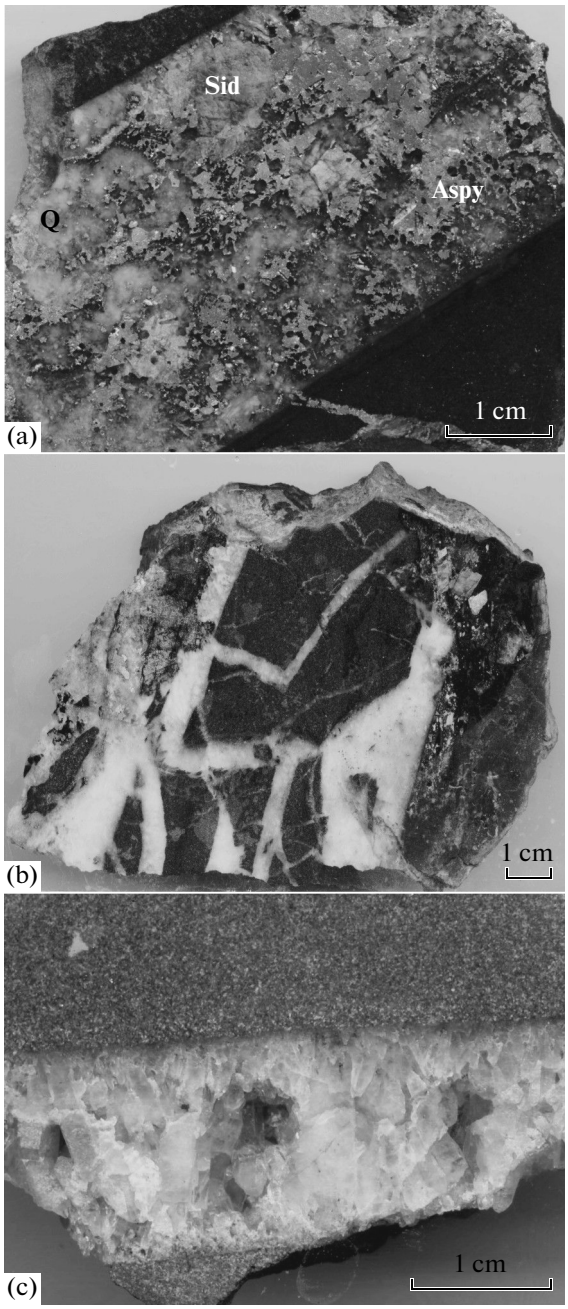

Fig. 3. Quartz–carbonate veinlets making up orebodies at Arkachan deposit: (a) quartz–siderite–polysulfide veinlet, (b) branching of quartz veinlets in crush zone, (c) veinlet of translucent druse-like quartz. Q, quartz; Sid, siderite; Aspy, arsenopyrite.

Bi-minerals are widespread in late assemblages of the main gold stage. They are represented by bismuth-

Table 1. Minerals of orebodies at Arkachan deposit

Abundance	Stages			
	Hydrothermal–metamorphic	Main gold	Silver–polymetallic	Silver–antimony
Major	Quartz, ankerite	Quartz, siderite, arsenopyrite, danaite, pyrite	Quartz, siderite, arsenopyrite, pyrite, ankerite	Quartz, calcite
Subordinate	Pyrite	Muscovite, pyrrhotite, chalcopyrite, glaucodot, sphalerite, tetrahedrite, native bismuth, aikinite, bismuthinite, gustavite, cosalite, pavonite, schirmerite, native gold, matildite, ankerite	Sphalerite, galena, freibergite, diaphorite, zoubekite	Stibnite
Rare		Galena, molybdenite, stannite, cassiterite, scheelite, wolframite, ingodite, chalcocite	Chalcostibite, pyrargyrite, miargyrite	Acanthite

Table 2. Chemical composition of carbonates from Arkachan deposit

Mineral	Ore zone	*n*	CaO	MgO	FeO	MnO	SrO	Total
Siderite I	o.z.2	7	0.33	3.35	51.06	3.01	n.d.	58.77
"	o.z.3	54	1.79	2.80	53.48	1.62	n.d.	59.70
"	o.z.4	5	3.29	3.77	51.08	0.84	n.d.	58.99
Siderite II		1	0.2	1.04	48.65	10.43	n.d.	60.32
Ankerite I		3	27.62	9.1	19.45	0.4	0.15	56.57
"	o.z.3	11	27.46	10.15	17.54	0.58	n.d.	55.73
"	o.z.4	2	24.91	4.67	23.01	0.56	n.d.	53.14
Calcite		2	53.21	0.5	1.46	0.27	0.61	56.04
"	o.z.3	6	51.28	1.17	n.d.	0.11	0.14	52.89

n, number of analyses; n.d., not detected, o.z., ore zone. Analyses have been performed at Laboratory of X-Ray Spectral Analysis, Diamond and Precious Metal Geology Institute, Siberian Branch, Russian Academy of Sciences (Camebax-Micro, analyst L.M. Popova).

inite, cosalite, gustavite, aikinite, matildite, schirmerite, and pavonite, which are frequently intergrown and associated with chalcopyrite.

Bismuthinite, the most abundant of Bi minerals at the deposit, is closely associated with chalcopyrite. Native gold frequently occurs just in this assemblage. Bismuthinite forms prismatic crystals (Fig, 4), intergrowths, or fan-shaped split grains in siderite among quartz, arsenopyrite, or pyrite aggregates. Bismuthinite constantly contains (wt %) Pb (0.3–2.8), Cu (up to 0.8), and Sb (up to 0.3). Tiny grains of *native bismuth*, a well as Pb–Bi and Ag–Pb–Bi sulfosalts are often identified in bismuthinite (Table 8).

Cosalite $Pb_2Bi_2S_5$ forms joint segregations with bismuthinite. The contents of major components vary within the following limits (wt %): 36.97–37.98 Pb, 44.92–45.89 Bi, and 15.34–17.64 S (Table 8). The chemical composition of cosalite is close to stoichiometric, although Cu, Ag, Fe, Sb, Se admixtures are frequently mentioned in the literature. It has even been suggested that the mineral stabilizes owing to these admixtures (Mozgova, 1985; Topa and Makovicky, 2010 and references therein).

Gustavite $AgPbBi_3S_6$ often occurs in ore zone 2, where it fills interstices in pyrite–arsenopyrite aggregates together with galena and chalcopyrite and makes up intergrowths with tetrahedrite and galena in chalcopyrite. Gustavite contains antimony (0.08–0.43 wt %) as an admixture. Microprobe results are recalculated to the formula $Ag_{0.94–1.01}Pb_{0.98–1.08}Bi_{2.87–2.91}Sb_{0.1–0.4}S_{6.04–6.11}$ (Table 8). No Sb admixture is noted in association with tetrahedrite.

Aikinite $PbCuBiS_3$ occurs as individual grains or intergrowths with bismuthinite in chalcopyrite frequently in association with native gold. According to microprobe data, the composition of aikinite corresponds to the formula $Pb_{1.06–1.07}Cu_{0.7}Bi_{1.12–1.14}S_{3.10–3.13}$ and does not contain admixtures (Table 8).

Matildite $AgBiS_2$ forms intimate ingrowths with galena I within chalcopyrite. Joint segregations with

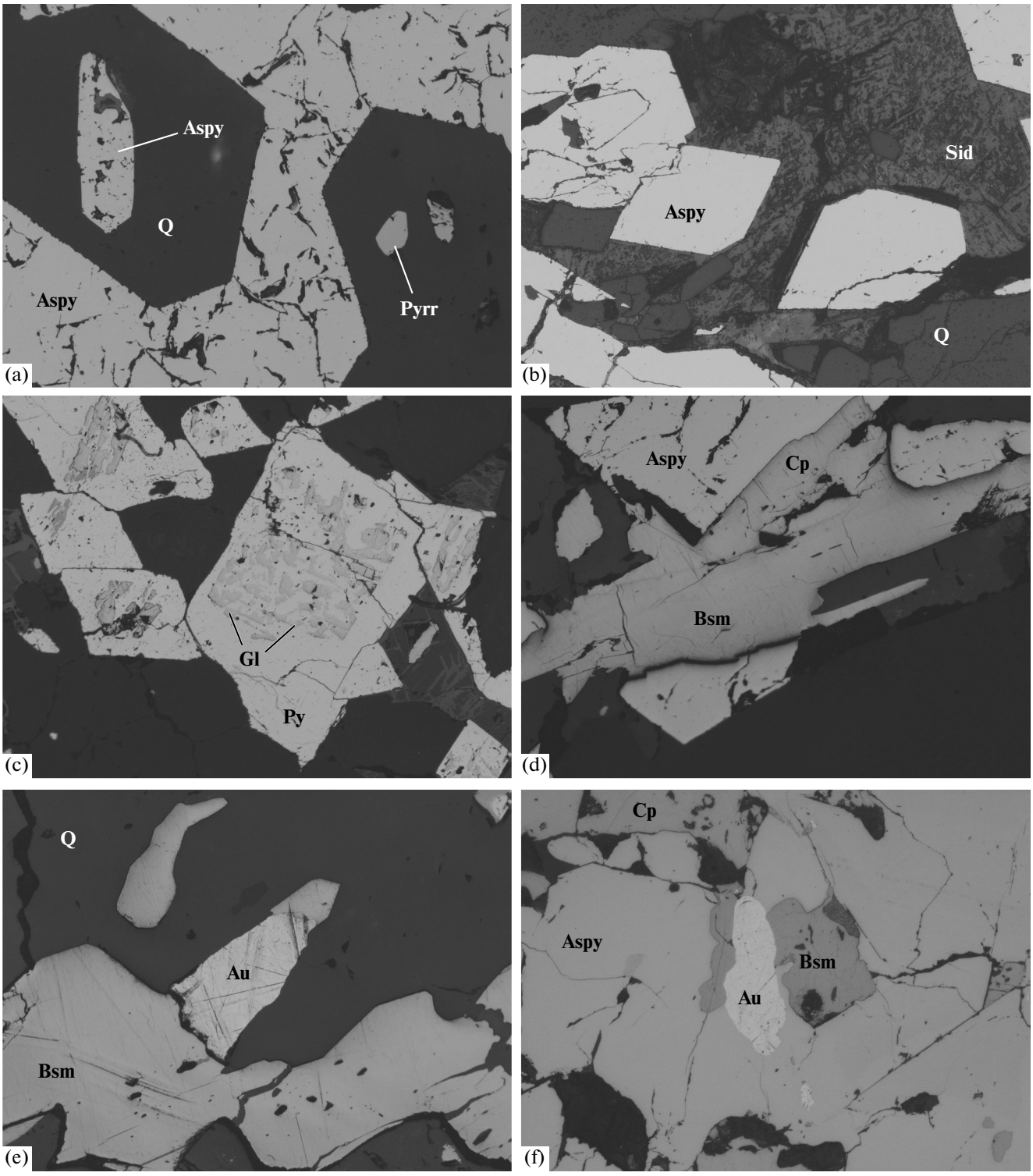

Fig. 4. Relationships between minerals of various assemblages at Arkachan deposit: (a) inclusions of arsenopyrite and pyrrhotite in quartz crystals; (b) flattened rhombic arsenopyrite crystals in siderite; (c) replacement of certain zones in pyrite crystals with galena; (d) bismuthinite and chalcopyrite in association with arsenopyrite; (e, f) native gold–bismuthinite intergrowth in quartz (e) and arsenopyrite (f). Q, quartz; Aspy, arsenopyrite; Pyrr, pyrrhotite; Sid, siderite; Gl, galena; Au, native gold; Bsm, bismuthinite; Cp, chalcopyrite.

Table 3. Trace element contents (ppm) in pyrite and arsenopyrite from Arkachan deposit: atomic absorption spectrosopy data

Element	Au				Ag–Pb	Au				Ag–Pb
	o.z.2	o.z.3	o.z.4	o.z.5		o.z.2	o.z.3	o.z.4	o.z.5	
	pyrite					arsenopyrite				
n	12	39	8	3	3	8	5	6	2	2
Au*	0.9	6.4	0.79	1.04	0.12	6.78	42.5	33.1	8.98	2.1
Ag*	805	941	874	945	2769	390	246	160	1395	2653
Co*	56	208	392	51	18	295	554	5733	490	89
Ni*	65	205	53	11	27	44	165	26.7	220	61
Sb*	64	37	32	17	54	171	183	63.3	446	736
Bi*	110	60	113	112	<30	288	204	3057	311	55
Cu*	5508	3445	620	3547	257	1789	601	120	424	132
Zn	53	21	135	15	267	12	14	50	76	112
Ga	0.3	0.4	0.5	0	0	0.2	0.2	0.2	0	0
As	335	113	45	110	86	»	»	»	»	»
Sn	4.4	1.4	4.4	18	12	0.9	1.2	8.5	9.2	37
W	0.5	0.4	0.6	0	0	0.5	0.5	0.6	0.5	<0.5
Pb	10	7.6	31	4	54	1.2	2.7	38	54	134

Stages: Au, main gold; Ag–Pb, silver–polymetallic. Analyses have been performed at Centergeoanalytica Company, Yakutsk (analysts T.Ya. Kovaleva, T.F. Gornaya, Z.P. Popova). * atomic absorption spectroscopy; *n*, number of analyses.

pavonite and schirmerite are noted. According to microprobe results, *pavonite* $AgBi_3S_5$ contains 4 wt % Pb. The concentrations of major components in *schirmerite* $AgPb_2Bi_3S_7$ vary as follows: 7.8–8.5 Ag, 21.2–28.2 Pb, 47.1–50.3 Bi, and 16.3–17.4 S (Table 8); Sb admixture (0.3–3.3 wt %) frequently occurs in schirmerite.

Native gold fills interstices and microcracks in arsenopyrite, joint segregations with bismuthinite or Ag–Pb–Bi sulfosalts in arsenopyrite (Fig. 4), and is associated with chalcopyrite. The fineness of native gold varies from 690 to 904‰ (Fig. 5). In addition to Ag (9.5–30.1 wt %), admixtures of Cu (0.01–0.04 wt %) and Sn (up to 0.04 wt %) are frequently detected. Up to 0.02 wt % Bi were revealed in certain gold grains, and Hg (up to 0.4 wt %) is detected sporadically. According to the results of quantitative spectral analysis, native gold contains (ppm): 12–50 Pb, 20–60 Te, 50–122 Bi, 65–214 Sb, 165–438 Cu, and 130–800 Sn. Native gold is nonuniformly distributed within orebodies and economic contours. Its concentrations vary from tenth fractions of g/t to 130 g/t. Gold grains are commonly fine; 80% of gold grains are 0.0*n* mm in size, and only single grains reach 1–2 mm. Gold grains are mainly round (droplike) or look like angular clots, wirelike and sheetlike with angular and denticulated outlines; perfectly faced gold grains are infrequent. The share of round grains increases with decrease in size.

Ingodite Bi_2TeS occasionally occurs in association with native gold. According to microprobe results, its formula is recalculated to $Bi_{1.74–1.75}Pb_{0–0.15}Te_{1.23–1.27}S_{0.86–1.00}$. Pb admixture (up to 5 wt %) is detected in some grains.

Ankerite II is insignificant in abundance and reveals the same tendency to lose Mg with depth as siderite (Table 2).

Silver–polymetallic Stage

Minerals pertaining to the silver–polymetallic stage fill fractures and cross-cutting veinlets in mineral aggregates of the early stage, as well as separate veinlets mainly at the northern flank of the ore field and in ore zone 5.

Siderite II occurs in veinlet selvages of this stage and, in contrast to Au-bearing veinlets, is characterized by high Mn contents (9–11 wt %).

Quartz III fills central parts of veinlets; its semi-transparent medium- to fine-grained aggregates contain clusters of ore minerals (pyrite, arsenopyrite, galena, sphalerite, and Ag–Pb–Sb sulfosalts, up to a few vol %).

Pyrite II makes up medium- to fine-grained aggregates in quartz. According to the results of emission and atomic absorption spectroscopy, pyrite II is characterized by markedly elevated Ag, Pb, Zn, Sb, and Sn concentrations (Table 3).

Arsenopyrite II forms monomineralic aggregates or intergrowths with pyrite in quartz. According to microprobe, arsenopyrite II contains (wt %): 33.6–

Table 4. Chemical composition (wt %) of sulfoarsenides from Arkachan deposit

Mineral	Fe	Co	Ni	Sb	As	S	Total
Arsenopyrite I	34.74	0.34	0.01	0.02	41.21	22.92	99.24
	34.79	0.05	0	0.04	42.11	22.17	99.16
	34.23	0.05	0.01	0.04	42.68	21.47	98.48
	34.4	0.16	0.01	0.05	43.9	21.35	99.87
Arsenopyrite II	34.57	0.06	0.01	0.02	44.04	21.57	100.27
	34.24	0.04	0.02	1.32	40.32	23.12	99.06
	33.6			2.1	39.9	23.1	98.70
	34.1			1.8	40.3	23.4	99.60
	34.59	0.06	0.01	0.03	43.53	21.24	99.46
	34.57	0.06	0	0.04	43.73	21.27	99.67
	34.55	0.06	0.01	0.04	43.82	21.24	99.72
	34.47	0.08	0.01	0.04	43.77	21.21	99.58
Danaite	21.72	11.35			44.72	21.15	98.94
	23.32	12.02			44.53	21.48	101.35
	21.66	14.41			43.95	20.23	100.25
	25.18	10.12			44.67	20.63	100.60
	30.28	6.06			43.77	20.6	100.71
Glaucodot	20.82	15.5			44.28	19.46	100.06
	19.35	16.11			44.15	20.46	100.07

34.6 Fe, 39.9–44.0 As, 21.2–23.4 S and is enriched in Sb up to 2.5; the S/As ratio varies from 1.13 to 1.36, i.e., is higher than in arsenopyrite I (1.14–1.30). As follows from the results of AAS, arsenopyrite II is enriched in Ag and Sb (Table 3).

Sphalerite II is yellowish and pale pink in color and fills interstices in pyrite–arsenopyrite aggregate. According to microprobe results, sphalerite II is low-Fe (0.*n*–1.6 wt %); i.e., its Fe mole fraction is much lower than of sphalerite I. Sphalerite II always contains 0.2–0.3 wt % Cd and 0.03–0.07 wt % Sn.

Galena II is widespread as dispersed disseminations, small clusters, and thin discontinuous chains within fine-grained quartz III. In contrast to galena I, galena II contains 0.2–0.4 wt % Ag and 0.2 wt % Sb (Table 6). It is probable that the limited solubility of silver in galena ($Pb^{2+} = 2Ag^{+}$) takes place along with isomorphism: $2Pb^{2+} = Ag^{+} + Sb^{3+}$.

Fahlore II, which is associated with galena II, sphalerite II, and arsenopyrite II, is a rare mineral. The Ag content in fahlore II varies from 17.1 to 23.7 wt % (Table 7). The microprobe results are recalculated to the formula $(Cu_{5.65–7.41}Ag_{2.85–4.56})_{10.10–10.40}(Fe_{0.05–1.15}Zn_{0.58–1.29})_{1.72–2.04}(Sb_{3.99–4.12}Bi_{0–0.01})_{3.99–4.12}S_{12.59–13.10}$ and to allow fahlore II to identify as Ag-tetrahedrite-freibergite (Mozgova, 1985).

Ag and Pb sulfoantimonites, among which *diaphorite* $Ag_3Pb_2Sb_3S_8$ and *zoubekite* $AgPb_4Sb_4S_{10}$ have been identified, occur as intergrowths with fahlore II and galena II. The chemical composition of diaphorite ($Ag_{2.83–3.27}Cu_{0.01–0.19}Pb_{1.81–2.00}Sb_{2.90–3.11}S_{7.77–8.15}$) is close to the theoretical composition and characterized by Cu (up to 0.9 wt %) and less frequently Bi (0.1 wt%) admixtures. Cu (0.3–2.1 wt %) and Zn (up to 0.6 wt %) have been revealed in zoubekite as admixtures (Table 8).

Chalcostibite ($Cu_{1.01}Sb_{0.99}S_{2.00}$) with insignificant Bi and Zn admixtures, as well as *pyrargyrite* and *miargyrite* have been identified as intergrowths with fahlore II and Ag–Pb–Sb sulfosalts.

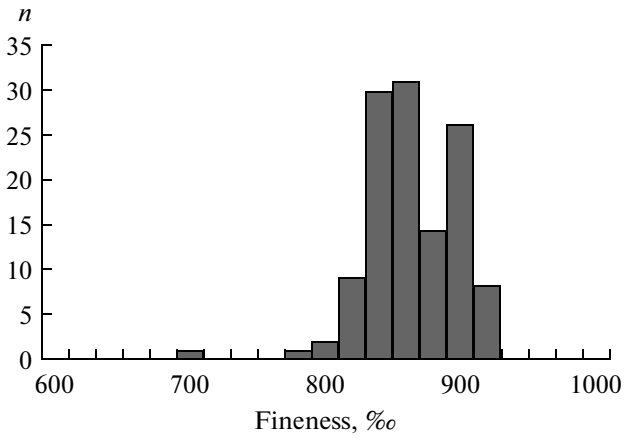

Fig. 5. Fineness of native gold at Arkachan deposit.

Table 5. Chemical composition (wt %) of sphalerite and stannite from Arkachan deposit

Mineral	Ag	Cu	Zn	Fe	Cd	Sn	S	Total
Sphalerite I	–	0.15	57.47	8.99	0.48	0.12	33.61	100.82
	–	0.01	60.44	7.29	0.16	0.01	33.40	101.31
	–	0.03	59.91	7.14	0.15	–	33.45	100.69
	–	1.51	58.92	7.78	0.16	–	32.72	101.09
	–	1.95	59.73	5.09	0.11	0.02	33.49	100.39
	–	1.51	58.92	5.78	0.16	–	32.72	99.09
	–	1.99	58.48	5.99	0.05	–	33.7	100.21
	–	1.71	57.77	6.28	0.06	0.03	33.24	99.09
	–	2.52	54.7	9.33	0.09	–	33.78	100.42
Sphalerite II	–	0.06	67.90	0.11	–	–	33.72	101.97*
	–	–	66.93	0.19	0.63	0.08	32.86	100.69
	0.04	–	67.37	0.05	0.31	0.03	33.3	101.10
	–	–	67.18	0.16	0.21	–	33.04	100.59
	0.14	–	66.23	–	0.76	0.21	33.21	100.55
	0.06	–	67.57	–	0.48	0.09	33.08	101.28
	0.04	–	66.15	–	1.53	0.06	32.46	100.24
Stannite	–	29.4	2.1	11.8	–	26.9	30.1	100.30
	–	29.7	2.2	11.0	–	27.2	30.2	100.30

*The analysis contains 0.18 wt % of Pb.

Table 6. Chemical composition (wt %) of galena from Arkachan deposit

Mineral	Ag	Pb	Sb	S	Total
Galena I		87.3		12.8	100.10
		86.74		13.23	99.97
		86.94		12.63	99.57
		87.35		12.66	100.01
		86.82		13.11	99.93
		86.89		13.12	100.01
Galena II	0.16	87.82	0.16	13.66	101.86*
		87.8		12.1	99.90
		87.6		12.6	100.20
	0.25	86.35	0.18	12.66	99.44
	0.19	86.3	0.14	12.8	99.43
	0.34	86.34	0.21	13.23	100.12
	0.41	86.56	0.23	12.63	99.83

*The analysis contains 0.06 wt % of Zn. Bi content is below detection limit in all analyses.

Silver–Antimony Stage

The silver–antimony mineralization in veins and veinlets of cryptogranular *quartz IV*, which has been found in ore zone 6 along with stibnite and less frequently acanthite within the intergranular space, is related to the final stage. Calcite is the latest mineral in this assemblage.

The mineralogy of ore zones and the sequence of mineral formation at the Arkachan deposit have no analogs among the known types of gold deposits in northeastern Russia. The predominance of siderite among gangue minerals is the main distinguishing feature. This mineral is not inherent to gold deposits but is widespread at cassiterite–sulfide and silver–polymetallic deposits. However, in contrast to the latter, where siderite is one of the earliest minerals, here it is a late mineral forming after quartz and sulfides.

The elevated amount of sulfides in ore (15–20 vol %, on average) is one more feature of the Arkachan deposit. Locally veinlets are completely composed of sulfides.

REE DISTRIBUTION IN ROCKS AND MINERALS

We studied REE distribution in host rocks, metasomatic rocks, carbonates and quartz from veins in ore zones, and fluid inclusions in quartz. Analyses were performed at the following laboratories: Institute of

Table 7. Chemical composition (wt %) of fahlore from Arkachan deposit

Mineral	Ag	Cu	Zn	Fe	Pb	Sb	As	Bi	S	Total
Fahlore I	4.3	36.3	1.9	4.4	–	28.1	–	–	24.7	99.70
(tetrahedrite)	5	34.9	2.5	5.1	–	27.9	–	–	24.7	100.10
	4.7	35.7	2.1	5.3	–	28	–	–	25.2	101.00
	5.97	34.89	5.95	1.31	0.01	25.82	0.56	–	24.67	99.18
	5.88	34.67	6.83	1.37	–	25.68	–	–	24.24	98.67
Fahlore II	17.8	26	4.7	2.5	–	27.7	–	–	22.5	101.20
(Ag-tetrahedrite–freibergite)	17.7	25.9	4.2	2.1	–	26.7	–	–	22.6	99.20
	17.1	26.1	4.1	2.7	–	27.5	–	–	22.8	100.30
	26.26	19.15	2.36	3.32	–	25.94	–	0.06	22.37	99.46
	23.69	19.93	6.39	0.15	–	26.47	–	0.06	21.81	98.50
	22.99	21.26	2.06	3.7	–	26.23	–	0.11	22.65	99.00

Geology of Ore Deposits, Petrography, Mineralogy, and Geochemistry, Russian Academy of Sciences (IGEM RAS) (carbonates, ICP-MS, analyst S.A. Gorbacheva); Institute of Tectonics and Geophysics, Far East Branch, Russian Academy of Sciences (ITG FEB RAS) (quartz, ICP-MS, analyst N.L. Berdnikov); Central Institute of Geological Exploration for Base and Precious Metals (TsNIGRI) (fluid inclusions, ICP-MS, analysts S.G. Kryazhev and Yu.V. Vasyuta); and IGEM RAS (rocks, neutron activation analysis, analyst A.L. Kerzin). Normalization to chondrites was used for visualization of results (Taylor and McLennan, 1985). Eu (Eu/Eu*) and Ce (Ce/Ce*) anomalies were calculated from formulas $Eu/Eu^* = Eu/(Sm^*(Tb^*Eu)^{1/2})^{1/2}$ and Ce/((2La + Sm)/3, chondrite-normalized values.

REE Distribution in Country Rocks

The REE contents in unaltered siltstones is twice as high as unaltered sandstones: 171.8 and 87.1 ppm, respectively. Siltstones are enriched in LREE (La/Yb = 7.1–11.1) and have a weak negative Eu anomaly (Eu/Eu* = 0.7–0.8).

In altered siltstones and sandstones, total REE contents increase and changes from 156 to 202 ppm and from 101 to 198 ppm, respectively. The highest total REE contents (826 ppm) have been established in a sample from Borehole 1 that penetrates altered siltstone of footwall of ore zone 3 (borehole 1) (Fig. 6). The concentrations of overall REE patterns increase in this sample as compared with that of the supraore sequence. An insignificant enrichment of altered siltstone in HREE relative to unaltered rocks has been established. In the sandstones that underwent sulfidation and contain quartz veinlents, the concentrations of all REE changed with increase in La/Yb ratio and insignificant positive Eu anomaly (Eu/Eu* = 1.4) appearance. The REE patterns in granitic rocks are rather homogeneous and the total concentrations are not high (58–69 ppm). All rocks are enriched in LREE, and their differentiation is insignificant.

REE Distribution in Carbonates

The REE contents in carbonates variable in age and composition from veins of several ore zones are given in Table 9. The highest total REE concentrations are detected in calcite (2838–2984 ppm); in ankerite they are 24.6–593 ppm and are minimal in siderite (3.1–124 ppm).

Preore ankerite I differs from ankerite II from Au-bearing veins in high REE contents (83–593 ppm) and is enriched in HREE. Differentiation of both LREE and HREE is insignificant. In carbonates from orebodies, the total REE concentrations markedly increase from early to late minerals (siderite → ankerite → calcite). In addition, a difference was revealed in REE distribution in carbonates from distinct ore zones. In siderite and ankerite from ore zone 2, REE concentrations are lower than in the same minerals from other zones.

In the ore zones themselves, REE distributions are correlated to mineral composition of veinlets (Fig. 7). In ore zone 3, siderite I from monomineralic veinlets is characterized by the prevalence of LREE over HREE. In siderite I from veinlets containing pyrite, arsenopyrite, and chalcopyrite, conversely, HREE dominate over LREE. In siderite I from pyrite–siderite veinlets, no distinctions have been revealed in behavior of LREE and HREE. In ore zone 2, siderites I from veinlets with abundant muscovite are characterized by La/Yb values both higher and lower than unity. Most likely, this is caused by the variable temperature of mineral formation. Enrichment in HREE proceeds at a lower temperature and is caused by the more efficient formation of HREE complexes under these conditions (Bau and Möller, 1992). The prevalent concentration of HREE rather than of LREE in siderite is caused by the "mineralogical effect" inas-

Table 8. Chemical composition (wt %) of Bi and Sb minerals from Arkachan deposit

Mineral	Ag	Cu	Zn	Fe	Pb	Sb	Bi	S	Total
Bismuthinite		0.65			2.58	0.17	78.32	19.40	101.12
		0.56			1.94	0.11	78.67	19.52	100.80
		0.02			0.36	0.13	79.66	19.15	99.32
		0.06			0.67	0.29	79.60	19.29	99.90
		0.05			0.40	0.11	80.02	19.46	100.05
		0.65			2.58	0.17	77.32	19.4	100.12
		0.56			1.92	0.06	78.71	19.19	100.44
		0.75			2.83	0.11	77.11	19.39	100.19
		0.56			1.94	0.11	78.67	19.52	100.80
		0.08			0.43	0.15	80.07	19.55	100.28
Cosalite					37.62		45.89	15.34	98.85
					36.97		45.12	17.64	99.73
					37.23		44.92	16.85	99.00
					37.46		45.63	16.42	99.51
					37.98		45.48	15.11	98.57
Gustavite	8.92				22.55		51.51	15.88	98.86
	9.34				20.13	0.30	54.16	17.53	101.46
	9.16				20.23	0.08	54.18	17.70	101.36
	9.76	0.10		0.01	18.17	0.43	54.41	17.34	100.22
Aikinite		7.43			36.57		38.67	16.38	99.05
		6.87			36.12		39.21	16.54	98.74
Schirmetite	8.14				25.12		50.32	16.33	99.91
	8.03				26.47		48.95	16.44	99.89
	7.82				25.91		49.84	16.29	99.86
	8.09				28.22	0.31	47.12	17.13	100.87
	8.21				21.17	3.12	50.02	17.35	99.87
	8.52				21.41	3.33	49.14	17.22	99.62
Pavonite	10.65	0.03		0.09	4.02		68.27	18.84	101.90
Diaphorite	26.21	0.89	0.1		27.81	26.62	0.11	18.51	100.25
	24	0.05			29.55	25.88	0.06	19.08	98.62
	22.86	0.08			30.32	26.26		19.15	98.67
	22.5	0.14	0.02		29.45	27.89		19.08	99.08
Zoubekite	8.75	2.11	0.59		42.88	26.78		18.68	99.79
	6.64	0.25	0.03		43.82	28.4		19.49	98.63
	6.1	0.27			44.65	28.45	0.04	19.43	98.94

much as LREE are larger and have a higher positive charge as Fe^{2+} (Bau and Möller, 1992).

Both almost horizontal REE patterns with positive Eu anomaly and the patterns with prevalent LREE and negative Eu anomaly are inherent to ankerite II from ore zone 3. The negative Eu anomaly in ankerite is caused by the interference of Mg^{2+} and Fe^{2+} replacement with large Eu^{2+} ion in the structure of this mineral.

Calcite is enriched in LREE, the LREE pattern is almost horizontal (La/Sm = 1.0–1.5), and HREE reveal significant differentiation (Gd/Yb = 6.5–14.4). A negative Eu anomaly (Eu/Eu* = 0.3–0.5) is revealed. This anomaly is probably caused by calcite crystallization from relatively low-temperature (<200°C) fluid.

The REE distribution in carbonates most likely is determined by physicochemical conditions of crystallization and "mineralogical effect." It is assumed that the mineral-forming fluid transformed REE patterns in altered rocks, and this does not allow us to suggest

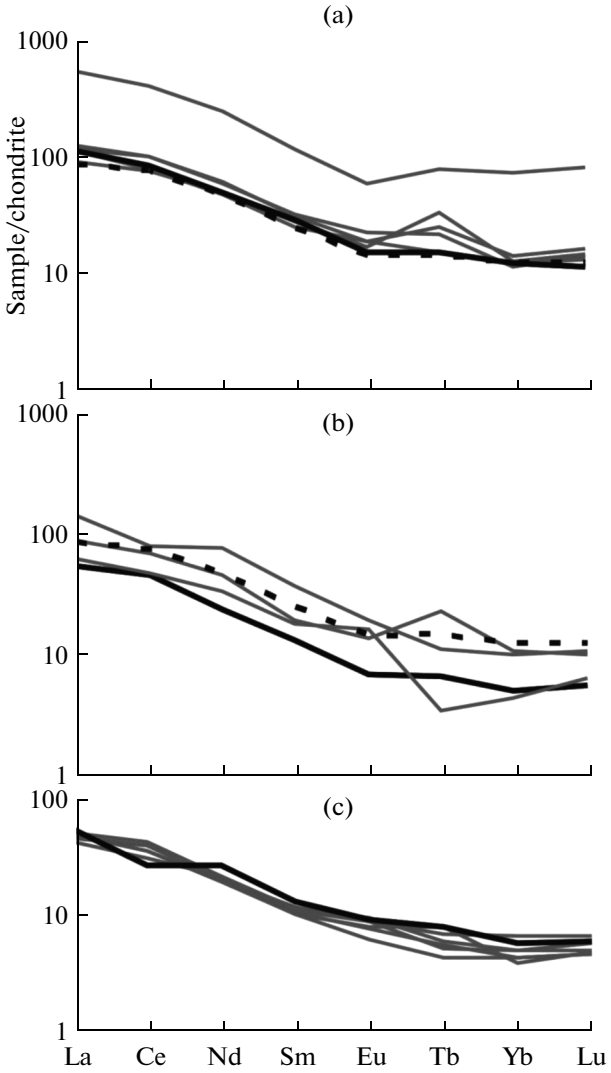

Fig. 6. Chondrite-normalized REE patterns for (a) siltstones, (b) sandstones, and (c) granitic rocks of Arkachan ore field. Unaltered rocks (a, b) and quartz porphyry dike (c) are shown in black. Dashed line denotes North American crystalline schist (NACS).

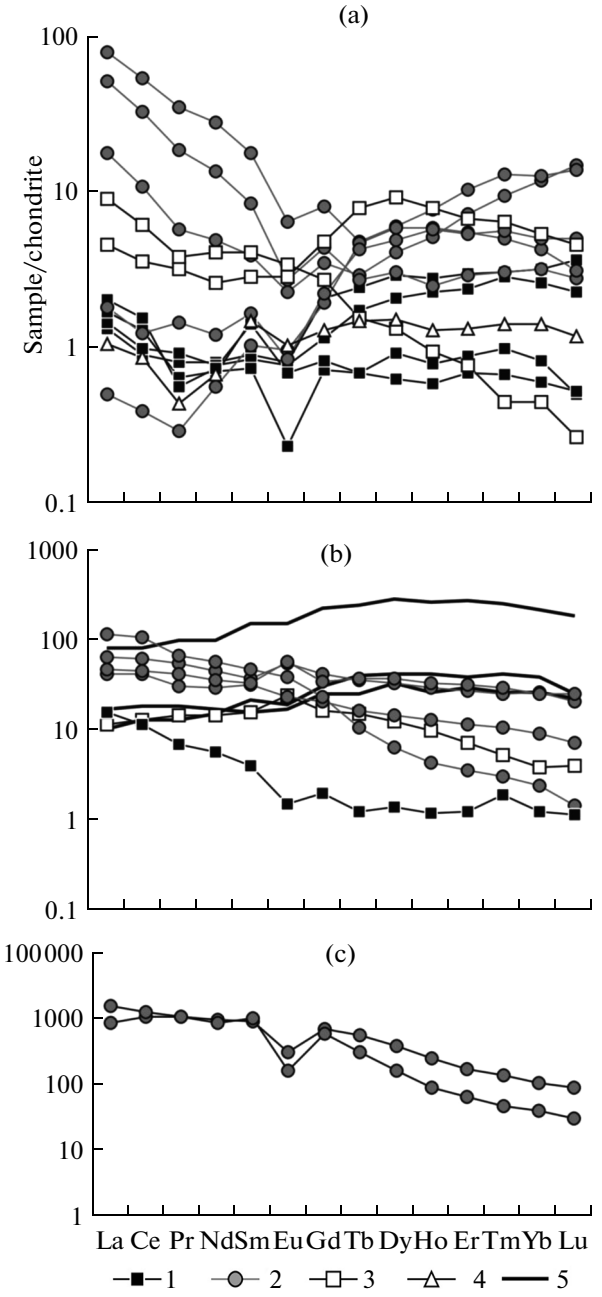

Fig. 7. Chondrite-normalized REE patterns of (a) siderite, (b) ankerite, and (c) calcite from Arkachan deposit. (1–3) main gold stage: (1) ore zone 2, (2) ore zone 3, (3) ore zone (4) silver–polymetallic stage, (5) hydrothermal–metamorphic stage.

that these chemical elements were recovered from host rocks.

REE Distribution in Quartz

Substantial variations of REE patterns in quartz have been revealed (Table 10). The total REE concentrations in this mineral vary from 4.4 to 17.8 ppm. There is insignificant enrichment in LREE (La/Yb = 1.3–6.9; ~1.5 is predominant). A moderate negative Eu anomaly (Eu/Eu* = 0.4–0.6) has been established except for quartz IV related to the Ag–Sb stage, where the Eu anomaly is slightly positive (Eu/Eu* = 1.2).

The REE patterns of various quartz generations from different ore zones are quite distinct (Fig. 8). The early milky-white barren quartz I is characterized by flat patterns with insignificant enrichment in LREE (La/Yb = 1.3–1.6) and a distinct negative Eu anomaly (Eu/Eu* = 0.5). The total REE concentrations are not high (4.4–6.1 ppm); LREE are only slightly differentiated (La/Sm = 1.3–1.4); HREEs are not differentiated at all (Gd/Yb = 1).

The total REE concentrations in quartz II of the main gold stage vary from 4.5 to 17.8 ppm. The REE patterns are more differentiated as compared with

Table 9. REE pattern parameters of carbonates from Arkachan deposit

Ore zone	*n*	Σ REE, ppm	Eu/Eu*	Ce/Ce*	La/Yb	La/Sm	Gd/Yb
Siderite I							
O.z.2	5	3.1–6.2	0.4–0.8	0.8–0.9	0.4–3.3	0.5–2.3	0.4–1.4
O.z.3	9	7.7–123.7	0.5–1.4	0.6–1.0	0.1–16.0	0.5–6.1	0.3–1.4
O.z.4	2	15.8–17.9	0.8–1.1	0.9	0.9–20.3	1.6–2.2	0.9–6.2
Siderite II							
O.z.2	2	4.1–5.6	0.8–1.0	0.7–1.0	0.8–4.9	0.7–2.7	0.9–1.3
Ankerite I							
	3	83–593	0.8–0.9	0.8–1.1	0.3–0.6	0.5–1.1	0.8–1.1
Ankerite II							
O.z.2	1	24.6	0.6	0.9	12.8	4.0	1.6
O.z.3	6	51.6–219.7	0.6–1.5	1.1–1.2	1.6–47.3	1.3–2.4	1.1–9.6
O.z.4	1	49	1.4	1.0	3.0	0.7	4.3
Calcite							
O.z.3	2	2838–2985	0.3–0.5	0.9–1.2	8.3–38.1	1.0–1.5	6.5–14.4

quartz I (La/Yb = 1.4–6.9). Negative Eu anomalies are distinguished by amplitude (Eu/Eu* = 0.4–1.0).

The REE patterns of quartz III related to the silver–polymetallic stage are close to the chondritic level; a negative Eu anomaly (Eu* = 0.6) is distinct.

Quartz IV of the silver–polymetallic stage is appreciably enriched in LREE (La/Yb = 5.2); HREE contents are close to the chondritic level. The total REE concentration is 9.5 ppm. A weak positive Eu anomaly (Eu/Eu* = 1.2) is noted. All studied quartz generations are devoid of Ce anomalies.

The REE patterns of quartz II from different ore zones are appreciably distinct. In quartz II from ore zone 4, REE contents depend on composition of veinlets. In quartz–sulfide veinlets the total REE contents are minimal and REE patterns are close to those of quartz I. In quartz II from quartz–carbonate veinlets, the total REE contents are maximal, primarily owing to enrichment in LREE.

The REE distribution in fluid inclusions from quartz at the Arkachan deposit was a subject of special study (Vikent'eva et al., 2012). The fluid contained therein is characterized by low total REE contents (1–4 ppm) and enrichment in LREE (LREE/HREE = 7.4–3.5). The REE patterns display Eu (Eu/Eu* = 0.3) and Ce (Ce/Ce* = 0.8–1.4) anomalies. The total REE concentrations in fluid inclusions diminish from early productive to late quartz generations.

Almost all samples are characterized by moderate negative Eu anomalies (Eu/Eu* = 0.4–0.6) (Fig. 9). Only in quartz IV, which fills thick veinlets, does the Eu anomaly become slightly positive (Eu/Eu* = 1.2–1.3). The negative Eu anomaly is typical of the fluids, which are derivatives of silicic magmas (Lüders et al., 1993) or of the high-temperature fluids (>200°C).

The total REE contents in altered rocks increases relative to unaltered varieties. The La/Yb ratio show that REE are absorbed by fluid in the process of rock alteration and formation of ore-bearing quartz veins. Crystallization of carbonates is accompanied by complex formation.

FLUID INCLUSIONS

Fluid inclusions were detected in quartz and siderite samples taken from the main ore zones of the deposit. Inclusions fit for microthermometric measurements were found in nine samples.

Fluid inclusions are small (1–30 μm). In accordance with known criteria (Roedder, 1984), primary and secondary inclusions are distinguished. The primary fluid inclusions are subdivided into three types by phase composition at room temperature (Fig. 10). Type I is represented by three-phase aqueous–carbon dioxide fluid inclusions containing liquid water as well as liquid and gaseous CO_2. Single-phase inclusions of type II are filled with gaseous dense carbon dioxide, which occurs in a liquid state at room temperature. These inclusions frequently contain a narrow rim of aqueous solution condensed by a cooling of inclusions. Inclusions of type III consist of a transparent liquid and a gas bubble. Fluid inclusions of types I and II make up clusters occasionally localized in the same growth zones of quartz, providing evidence for their synchronous entrapment. Thus, quartz of ore veins crystallized under conditions where two immiscible fluids coexisting in the system apparently were products of aqueous–carbon dioxide–salt fluid separation into two phases: substantially liquid and substantially gaseous. Primary inclusions of type III were identified

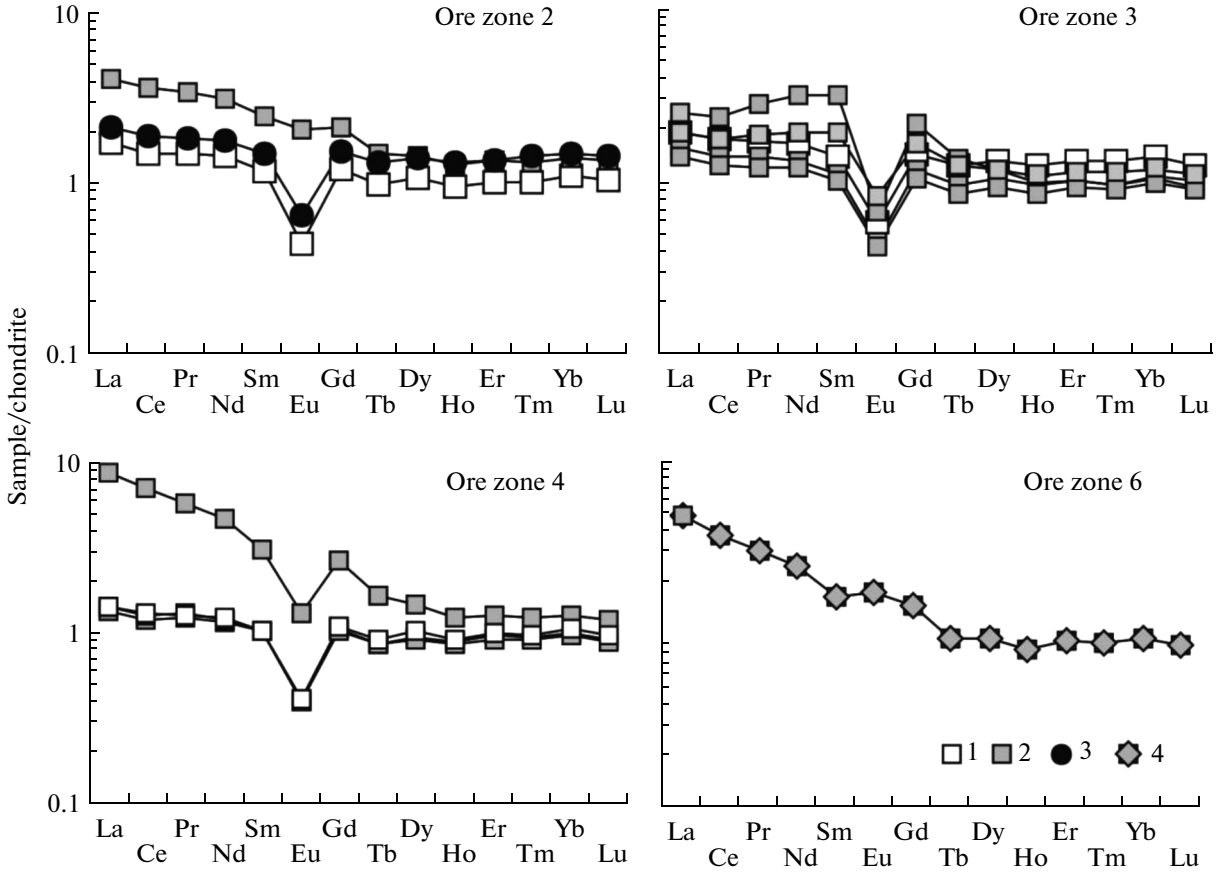

Fig. 8. Chondrite-normalized REE patterns of quartz from Arkachan deposit. (1) quartz I, (2) quartz II, (3) quartz III, (4) quartz IV.

in siderite and late quartz of ore veins, whereas secondary inclusions are contained in early quartz.

Individual inclusions were studied using a microthermometric system consisting of a LINKAM THMSG 600 chamber (Great Britain) with an 80× long-focus objective lens Olympus (Japan) installed on an Amplival microscope (Germany), video camera, and control computer. The accuracy of temperature measurements is ±0.2°C within temperature interval from –20 to +20 °C and falls at higher and lower temperatures. The composition of salts dominating in aqueous solutions was estimated from the melting temperature of eutectic (T_{eut}) (Borisenko, 1977). The total concentration of salts in fluid inclusions of type I was assessed from the melting temperature of gas hydrate and in fluid inclusions of type III from the melting temperature of ice based on experimental data for the NaCl–H_2O system (Bodnar and Vityk, 1994). The concentration of carbon dioxide and fluid density in individual inclusions was estimated based on volumetric relationships between various phases (Prokofev and Naumov, 1987). Pressure was determined by the intersection of isochore and isotherm (Kalyuzhny, 1982) obtained from the results of studying fluid inclusions of types I and II. Salt concentrations, fluid density and pressure were estimated using FLINCOR program (Brown, 1989).

The bulk analysis of fluid-filling inclusions was carried out from a probe 0.5 g in mass, fraction 0.5–0.25 mm at Central Institute of Geological Exploration for Base and Precious Metals (TsNIGRI), analyst Yu.V. Vasyuta; the technique used was described by Kryazhev et al. (2006). The amount of water necessary to calculate concentrations of elements in fluid was determined preliminarily from the same probe. The carbon dioxide, methane, cation, and anion compositions of fluid were analyzed, and the ICP-MS method was used to determine a wide range of ore, rare, and dispersed elements.

Microthermometric Study

The results of studying 259 individual fluid inclusions by heating and cooling of preparations are presented in Table 11 and Fig. 11. The primary fluid inclusions of type I in quartz II were homogenized at temperatures of 385 to 279°C (Table 11). The temperature of CO_2 melting in these inclusions varied from –57.4 to –58.8°C, i.e., is lower than melting point of pure CO_2 (–56.6°C) and can indicate an admixture of low-boiling gases, e.g., methane. Gas

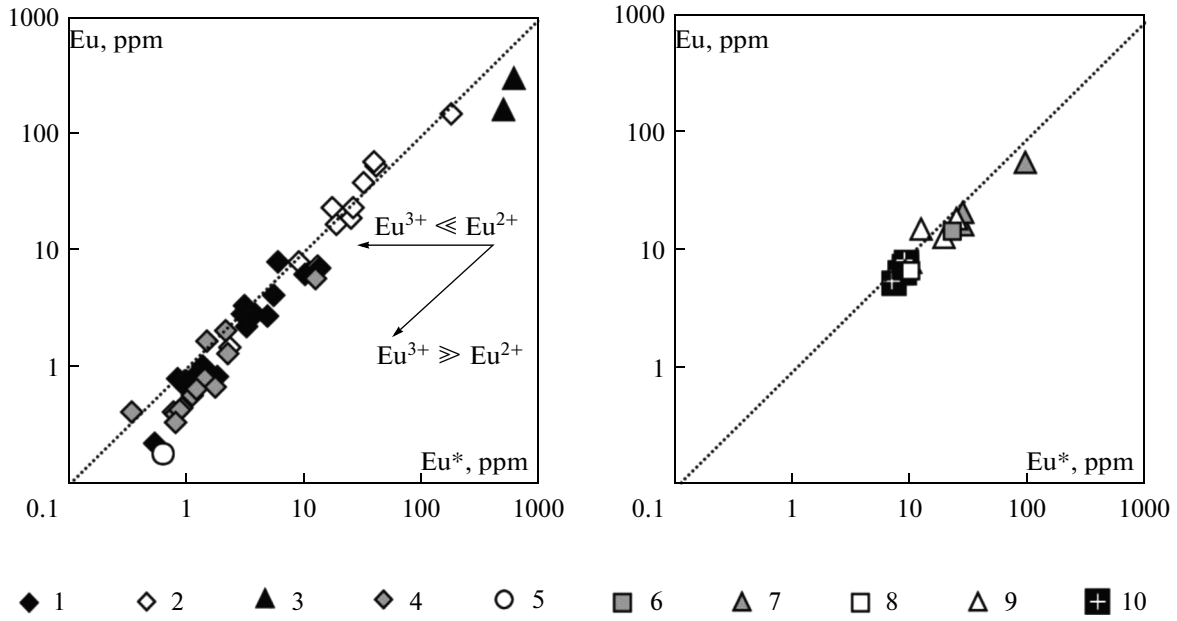

Fig. 9. Redox parameters of hydrothermal fluid at Arkachan deposit. (1–3) carbonates: (1) siderite, (2) ankerite, (3) calcite; (4) quartz, (5) fluid inclusions in quartz; (6, 7) siltstone: (6) unaltered, (7) altered; (8, 9) sandstone: (8) unaltered, (9) altered; (10) altered granite porphyry.

hydrate melted at temperature from +4.2 to –10.2°C. The salinity of the fluid captured by inclusions of this type estimated on the basis of these data varies from 18.8 to 26.2 wt % NaCl equiv. The concentration of carbon dioxide in the fluid of inclusions changed from 3.6 to 1.3 mol/kg of solution (fluid density varies from 1.07 to 0.84 g/cm^3).

The homogenization of carbon dioxide into a liquid phase in fluid inclusions of type II took place at temperatures of +16.5 to +29.5°C. Carbon dioxide melted from –57.6 to –59.6°C, i.e., somewhat lower than melting temperature of pure CO_2 (–56.6°C). This implies that small amounts of methane or nitrogen occur in the gas phase. The density of the gaseous phase is rather high (0.64–0.81 g/cm^3).

Primary fluid inclusions of type III are homogenized in liquid at 261–324°C (Table 11). The first portions of the liquid arose after complete freezing (eutectic temperature) at –32 to –46°C. This shows that dissolved Na and Ca chlorides dominate in aqueous salt solution. The temperature of ice melting varied from –2.2 to –5.8°C; these values correspond to salt concentrations from 3.7 to 9.0 wt % NaCl equiv. The density of these fluids varies from 0.70 to 0.86 g/cm^3.

Primary fluid inclusions of type III in siderite are homogenized into liquid at 281–283°C (Table 11). The eutectic temperature (–48°C) indicates that dissolved Na and Ca chlorides are predominant in aqueous salt solution. The temperature of ice melt is –9.5°C and corresponds to a salt concentration of 9.5 wt % NaCl equiv. The fluid density is 0.88–0.89 g/cm^3.

The secondary fluid inclusions of type III homogenized into liquid at 200–269°C (Table 11). The eutectic arose at temperature from –41 to –53°C. Thus, dissolved Na and Ca chlorides occur in aqueous salt solution. Temperature of ice melt varies from –16.2 to –23.0°C. In some inclusions hydrohalite is dissolved at –3.9°C, and this corresponds to the solution salinity of 19.8 to 22.6 wt % NaCl equiv. The density of solution changed from 0.97 to 1.03 g/cm^3.

The homogenization temperature of primary fluid inclusions of type I is regarded by us as a temperature of quartz crystallization, because with the capture of fluid inclusions under conditions of fluid phase separation, i.e., in the line of two-phase equilibrium, the correction to effect of pressure is not required (Roedder, 1984). Thus, quartz II was formed within a temperature interval of 385 to 280°C. The fluid pressure estimated for this temperature changed in the course of phase separation from 1830 to 1060 bar (Table 11). It should be noted that the pressure, under which quartz II was formed, increases with depth.

Analysis of Water and Gas Extracts from Fluid Inclusions in Quartz

The bulk composition of fluid inclusions was analyzed in 13 samples of several quartz generations from ore veins at the deposit (Table 12) and from different zones with ore mineralization. In general, the bicarbonate–sodium chloride fluids of main gold stage are the most mineralized.

The highly mineralized fluid from quartz IV of the silver–antimony stage substantially differs from other fluids in major components, in particular, in the predominance of HCO_3^- and Ca. Fluid from quartz III of the silver–polymetallic stage is close to the latter, but Na and Cl concentrations are also rather high. The fluid of the gold-ore stage is characterized by the substantial contribution of CH_4 (CO_2/CH_4 = 6–109), whereas at other stages CO_2/CH_4 = 74–522; i.e., CO_2 dominates in the gas phase.

The microcomponent contents in fluids of each stage are also specific. Fluid from quartz I is characterized by a very low total content of microcomponents (604 mg/kg H_2O); 40% of them fall on ore elements and one third on Zn. The main contribution (mg/kg H_2O) belongs to B (158), Br (75), Sr (67), and Ba (53). The total content of trace elements in fluids from quartz IV is somewhat higher, and concentration of ore elements increases up to 75% of the total; As, Fe, Mn, and Sb are the most significant. The total content of trace elements in fluid inclusions from quartz III increases almost three times (75% fall on ore elements and more than half on Zn). The list of ore elements in this fluid is rather wide. These elements are fixed in proper mineral or in isomorphic admixtures in minerals. Fluid from inclusions in quartz II contains a maximum of trace elements, however, the role of ore elements is comparable with fluids from quartz I. The high Li content in fluid attracts attention. One third of total admixtures fall on this element, although the Li_2O content in quartz from main gold stage is 4–5 times lower than in quartz of Ag–Pb and Ag–Sb stages. Of ore elements in fluid from quartz II, As, Zn, Fe, and Mn play the most substantial role. In general, the list of trace elements completely coincides, and this probably is evidence for the commonness of their source.

The K/Rb ratio in fluid from inclusions in quartz II varies from 134 to 270; in quartz III this ratio is 81–263. These values generally correspond to K/Rb ratio for magmatic fluid related to granitic source (150–350, 230 on average) (Irber, 1999). The high ratio of these components (309–398) in inclusions from metamorphic quartz I and especially from cryptogranular quartz IV (803) shows a significant contribution of fluids from other sources.

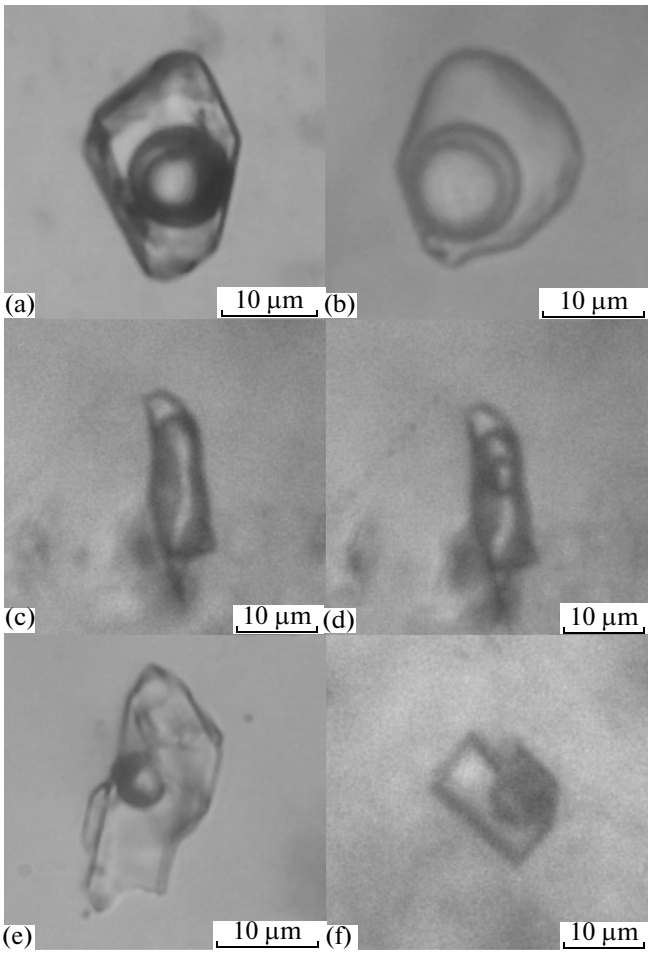

Fig. 10. Primary fluid inclusions in quartz (a–e) and carbonate (f) from ore veins at Arkachan deposit: (a, b) carbon dioxide–water, type I; (c, d) substantially gaseous inclusion of type II with carbon dioxide: (c) 20°C and (d) 12°C; (e, f) two-phase gas–liquid, type III.

GEOCHEMISTRY OF STABLE ISOTOPES

Stable Isotopes (O, C, S) in Minerals

The isotopic compositions of oxygen in quartz, oxygen and carbon in carbonates, and sulfur in sulfides were studied for various stages of ore formation. Monofractions of minerals pertaining to certain generations were carefully picked out under a binocular microscope. The measurements were carried out on mass spectrometers at the Laboratory of Isotopic Geology and Geochronology of IGEM RAS (analyst A.S. Avdeenko), the Laboratory of Stable Isotopes of the Far East Geological Institute, Far East Branch, RAS, and the Center of Isotopic Research of Russian Geological Research Institutein Petersburg. The possibility of using the results obtained as one selection was verified by control analyses of the same samples at different laboratories; 10 quartz and 9 carbonate samples have been duplicated. The error between laboratories for $\delta^{18}O$ is 0.1–0.7‰, and 100% convergence of results has been noted for half of samples. As concerns $\delta^{13}C$, only two samples differ by 0.4–0.5‰. No systematic errors in determinations have been revealed between laboratories.

In total, 54 quartz, 56 carbonate, and 112 sulfide samples (74 pyrite, 18 arsenopyrite, 15 chalcopyrite, 2 galena, 2 marcasite, 1 sphalerite) have been analyzed from veins localized in different ore zones of the deposit.

Oxygen isotopic composition of quartz. The early milky-white quartz I is characterized by $\delta^{18}O = +15.6 \pm 0.2$‰ ($n = 7$); $\delta^{18}O$ of quartz II associated with sider-

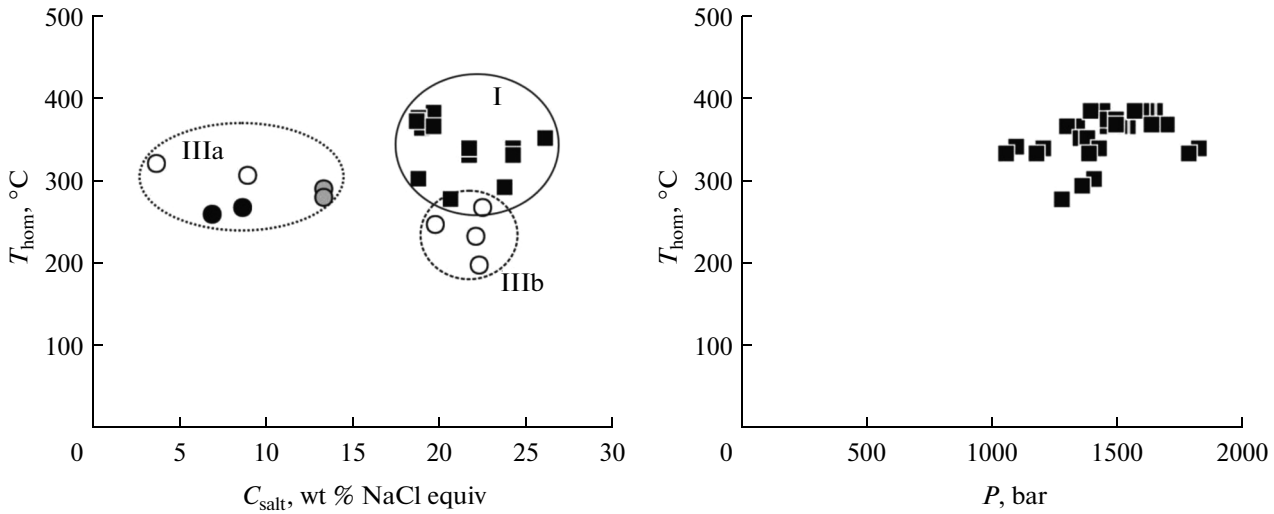

Fig. 11. *PT* parameters and composition of ore-forming fluids at Arkachan deposit. (I) carbon dioxide–water fluid inclusions in quartz, (IIIa) aqueous salt solution: primary inclusions in quartz, (IIIb) secondary inclusions in ore quartz. Black and white circles are inclusions in quartz I and quartz II, respectively; gray circles are inclusions in siderite I.

ite, native gold, and sulfosalts varies from +13.6 to +16.3‰ (n = 36). A wider $\delta^{18}O$ interval is noted for the main productive ore zones 3 and 4 toward enrichment in the light oxygen isotope. The $\delta^{18}O$ values of chalcedony-like quartz III varies from +14.7 to +17.3‰ (n = 6), whereas the very narrow range from +8.9 to +9.4‰ (n = 5) is inherent to cryptogrtanular quartz IV.

Oxygen and carbon isotopic compositions of carbonates. The $\delta^{18}O$ for siderite I of main gold stage varies from +13.6 to +17.7‰ (n = 28) (Fig. 12). Later ankerite II is insignificantly enriched in the light oxygen isotope: $\delta^{18}O = +14.3 \pm 0.3$‰ ($n$ = 9). The oxygen isotopic composition of siderite II at the silver–polymetallic stage is similar to that of siderite I ($\delta^{18}O = +15.7 \pm 0.3$‰, n = 3). The oxygen isotopic composition of calcite associated with cryptocrystalline quartz IV at the silver–polymetallic stage is markedly distinct. It is enriched in light oxygen isotope ($\delta^{18}O = +7.2 \pm 0.3$‰, n = 2).

Carbon isotopic compositions of different carbonate generations are markedly distinct. The $\delta^{13}C$ values for siderite I and ankerite II of main gold stage are −6.0 to −3.0‰ and −5.1 to −3.6‰, respectively. The lower $\delta^{13}C$ = −6.2 to −7.2‰ are characteristic of siderite II at the silver–polymetallic stage. The $\delta^{13}C$ of calcite is -3.5 ± 0.1‰.

Ankerite I is enriched in the heavy carbon isotope ($\delta^{13}C$ = −2.2 to −1.0‰, n = 7); however, oxygen isotopic composition is similar to that of late carbonates ($\delta^{18}O$ = +12.9 to +15.3‰).

Sulfur isotopic composition of sulfides was studied for main gold veins from different ore zones at the deposit and a rather wide range of $\delta^{34}S$ from −5.7 to +16.0‰ has been obtained. Sulfides of early generations are distinguished by $\delta^{34}S$, varying from +1 to +16‰ for arsenopyrite I (n = 16) and −5.7 to +7.2‰ for pyrite I (n = 63). Sulfur isotopic compositions of late sulfide generations vary from −2.2 to +14.6‰ for chalcopyrite (n = 15), +0.5‰ for galena I, and +0.9‰ for sphalerite I. In addition, pyrite and arsenopyrite from zones of wall-rock sulfidation and marcasite nodules in host rocks ($\delta^{34}S$ = +4.3...+9.3, n = 2) have been analyzed. Intervals of $\delta^{34}S$ values for pyrite (0 ± 3.8‰) and arsenopyrite (9 ± 0.2‰) from altered rocks overlap intervals for the same minerals from veins, however, the former are narrower. Galena II of silver–polymetallic interval is characterized by ($\delta^{34}S$ = −0.6‰). It should be noted that pyrite I that replaces pyrrhotite I enriched in the light sulfur isotopes and this is expressed in low $\delta^{34}S$ for pyrite from ore zones 2 and 4, where pyrrhotite is widely replaced with pyrite–marcasite aggregate.

O, C, and S Isotopic Compositions of Mineral-Forming Fluid

The oxygen isotopic composition of fluids is calculated in accordance with equations of fractionation in hydrothermal systems using measured $\delta^{18}O$ and homogenization temperature of fluid inclusions in quartz and carbonate. It is assumed that in the quartz–H_2O, siderite–H_2O, ankerite–H_2O, and calcite–H_2O systems, the isotopic equilibrium between deposited minerals and hydrothermal fluid is set in at the temperature of mineral formation and then maintained after crystallization. The following equations were used for calculations (Zhang et al., 1989; Zheng, 1999), where T is Kelvin temperature:

$$\Delta_{quartz-H_2O} = \delta^{18}O_{quartz} - \delta^{18}O_{H_2O} = 3.306(10^6/T^2) - 2.71, \quad (1)$$

Table 10. REE distribution in quartz from Arkachan gold deposit

Sample	La	Ce	Pr	Nd	Sm	Eu	Gd	Tb	Dy	Ho	Er	Tm	Yb	Lu	Total	Eu/Eu*	Ce/Ce*	La/Yb	La/Sm	Gd/Yb
Ore zone 2																				
ark 2	0.64	1.46	0.21	1.03	0.28	0.04	0.38	0.06	0.41	0.08	0.26	0.04	0.28	0.04	5.19	0.51	0.98	1.55	1.44	1.10
ark 85	1.51	3.53	0.48	2.23	0.57	0.18	0.67	0.09	0.56	0.11	0.34	0.05	0.36	0.05	10.73	0.99	1.03	2.86	1.66	1.51
ark 100	0.79	1.81	0.26	1.27	0.35	0.06	0.48	0.08	0.54	0.12	0.35	0.05	0.37	0.06	6.59	0.56	0.97	1.44	1.42	1.04
Ore zone 3																				
ark 13-190	0.72	1.70	0.24	1.19	0.33	0.05	0.44	0.07	0.50	0.11	0.33	0.05	0.35	0.05	6.13	0.53	1.00	1.39	1.38	1.03
ark 17-58	0.92	2.18	0.28	1.24	0.29	0.03	0.38	0.05	0.36	0.06	0.21	0.02	0.21	0.02	6.25	0.42	1.09	3.01	1.96	1.49
ark 556-1	0.92	2.26	0.39	2.27	0.73	0.06	0.68	0.08	0.45	0.09	0.26	0.03	0.26	0.04	8.51	0.39	0.86	2.37	0.79	2.10
ark 320-1	0.58	1.36	0.19	0.94	0.26	0.04	0.36	0.06	0.40	0.08	0.25	0.03	0.27	0.04	4.86	0.52	1.00	1.44	1.40	1.08
ark 70-2	0.52	1.20	0.17	0.86	0.24	0.04	0.32	0.05	0.36	0.07	0.23	0.03	0.25	0.03	4.36	0.53	0.97	1.44	1.39	1.04
ark 70	0.71	1.70	0.26	1.40	0.44	0.07	0.51	0.07	0.46	0.09	0.28	0.04	0.29	0.04	6.37	0.59	0.92	1.65	1.01	1.43
Ore zone 4																				
ark 517-1	0.51	1.18	0.17	0.87	0.25	0.04	0.34	0.05	0.38	0.08	0.25	0.04	0.26	0.04	4.44	0.51	0.96	1.33	1.29	1.05
ark 516-2	3.29	6.97	0.83	3.49	0.74	0.12	0.84	0.10	0.58	0.11	0.33	0.05	0.32	0.05	17.82	0.61	1.03	6.85	2.78	2.10
ark 31	0.55	1.27	0.18	0.88	0.25	0.04	0.33	0.05	0.36	0.08	0.23	0.03	0.25	0.04	4.54	0.51	0.98	1.50	1.41	1.08
ark 53	0.54	1.29	0.18	0.91	0.25	0.04	0.35	0.06	0.41	0.08	0.26	0.04	0.27	0.04	4.72	0.51	1.00	1.35	1.37	1.04
Ore zone 6																				
ark 112	1.78	3.55	0.41	1.73	0.38	0.15	0.45	0.05	0.35	0.07	0.23	0.03	0.23	0.03	9.45	1.19	0.98	5.22	2.95	1.57

Table 11. Results of thermo- and cryometric study of individual fluid inclusions in quartz and carbonate from ore veinlets at Arkachan deposit

Sample	Inclusion type	n	T_{hom}, °C	T_{eut}, °C	$T_{ice\ melt}$ (NaCl), °C	$T_{melt CO_2}$, °C	$T_{hom\ of\ gas}$, °C	$T_{melt,gas\ hydr}$, °C	C_{salt}, wt % NaCl equiv	C_{CO_2}, mol/kg sol	C_{CH_4}, mol/kg sol	d, g/cm^3	P, bar	$(P_{H_2O} + P_{gas})/P_{H_2O}$
Quartz														
556015	1 P	25	385–366	–42...–44	–25.2 (–12.9) ...–20.3	–58.1...–58.7	25.4...28.6 G	0.2–1.3	18.9–19.7	3.6–3.0	0.4–0.3	0.88–0.96	1270–1650	6.0–8.1
	2 P	33	–	–	–	–57.9...–59.7	25.0...28.5 L	–	–	–	–	0.64–0.71		
	2 P	2	355 G	–41	–4.8	–58.5	28.0 L	1.1	–	–	–	0.66	1340	7.1
	3 S	6	269	–44	–23.0(–3.9)	–	–	–	22.6	–	–	0.97	–	–
Ark-70-2	1 P	22	374–353	–31...–42	–16.2 (+7.1) ...–16.5	–56.6...–57.2	27.6... 29.0 G	0.6–2.0	18.8–26.3	2.7–2.4	0.4–0.3	0.84–0.91	1500–1350	7.1–8.5
	2 P	10	–	–	–	–56.9...–57.2	26.4 26.9 L	–				0.68–0.69		
	3 S	17	235–200	–41...–42	–22.3...–22.8	–	–	–	22.2–22.4			1.00–1.03	–	–
Ark-9	1 P	4	368	–49	–16.3	–57.3	27.3 G	2.6	19.7	2.0	0.3	0.93	1700–1500	8.8–7.7
	2 P	16	–	–	–	–57.5	22.4...25.9 L	–	–			0.75–0.70		
	3 S	13	250	–53	–16.4	–	–	–	19.8			0.97		
Ark 17-58[1)]	3 P	19	269–261	–32...–33	–5.6... –4.3	–	–	–	8.7–6.9	–	–	0.86–0.85	–	–
Ark 31	3 P	11	324–309	–42...–46	–2.2... –5.8	–	–	–	3.7–9.0			0.70–0.80	–	–
Ark13-207	1 P	17	341–334	–39	–21.1	–57.3	28.9 G	–0.9	21.8	1.4	0.2	1.01	1830–1150	8.6–17.1
	2 P	13	–	–	–	–57.7...–57.9	16.5...28.1 L	–	–			0.81–0.65		
Ark 5173	1 P	8	342–333	–42	–23.9	–57.4	28.8 G	–0.8	24.3	1.3	0.2	1.03	1100–1060	7.7–8.3
	2 P	4	–	–	–	–57.6	29.5 L	–	–	–	–	0.62		
Ark 79	1 P	25	304–279	–33...–41	–19.3...–24.1	–57.7...–58.8	26.7...28.5 G	4.2...–10.2	18.9–23.8	3.1–1.4	0.5–0.1	0.94–1.07	1410–1280	16.4–21.7
	2 P	3	–	–	–	–59.6	21.1 L	–	–	–	–	0.76		
Carbonate														
Ark 13-206	3 P	11	293–281	–48	–9.5	–	–	–	13.4	–	–	0.88–0.89	–	–

Phase type of fluid inclusions: 1, carbon dioxide–water; 2, substantially gaseous carbon dioxide; 3, two-phase (gas–liquid) aqueous solution. Genetic types of inclusions: P, primary, S, secondary. n, number of studied inclusions; d, fluid density; L, homogenization of dense gas into liquid; G, homogenization into gas. [1]) preore hydrothermal-metamorphic quartz.

Table 12. Chemical composition of fluid inclusions in quartz from Arkachan deposit

Component	Main gold stage					
	ore zone 2	*ore zone 3*			*ore zone 4*	
	Ark 11	A-70	A-556-1	Ark 553-1	Ark 31	A-53
H_2O, ppm	551	743	947			347
Macrocomponents, g/kg water						
CO_2	53.02	26.46	37.35	9.03	3.85	22.63
CH_4	1.59	0.24	1.18	1.39	0.47	1.12
Cl^-	27.39	12.21	44.37	9.69	1.2	36.20
SO_4^{2-}	1.81	–	–	–	–	–
HCO_3^-	–	36.60	65.61	58.62	35.65	123.00
F^-	1.81	n.a.	n.a.	n.a.	n.a.	n.a.
Na	7.13	16.79	48.75	16	10.9	55.65
K	1.98	3.52	4.30	4.18	2.21	8.61
Ca	1.50	2.03	1.92	7.89	0.78	6.48
Mg	0.04	0.45	0.25	0.33	0.3	1.04
Microcomponents, 10^{-3} g/kg water						
Br	–	11	877	111	–	302
As	1222	45	54	260	38.4	71
B	82.64	239	342	356	267	1147
Li	5.31	635	830	1659	2441	1311
Rb	14.76	14.2	21.6	15.5	10.2	39.8
Cs	0.82	0.8	1.6	1.11	0.84	2.5
Mo	–	–	0.1	17.1	0.12	–
Sb	12.35	18.2	15.2	13.8	24	14.0
Sr	–	42	138	100.2	59	223
Mn	19.28	23	143	572	47.2	173
Cu	–	22	106	134	296	232
Zn	40.85	112	257	600	425	255
Cd	0.04	–	1.1	2.01	1.2	6.0
Pb	–	5.4	3.1	19.3	21.8	14.9
Bi	–	0.1	0.2	1.18	–	0.3
Ba	17.65	14	44	0.07	0.24	104
U	–	0.1	–	–	–	–
W	–	14.0	6.5	27	5.04	3.9
Ag	–	3.7	0.7	0.57	1.21	3.3
Au	–	2.2	0.9	11.3	–	–
Co	–	0.6	2.2	3.25	1.2	2.0
Ni	2.74	32	196	23.5	10.8	373
V	–	6.9	3.7	2.22	10.3	5.9
Cr	–	10.6	8.8	21.2	1.32	8.0
Tl	0.07	–	0.4	0.21	0.36	0.5
Sn	–	3.6	2.4	2.63	2.88	7.9
Hg	0.45	1.15	0.18	6.9	–	0.57
Ge	n.a.	í.î.	í.î.	9.4	12.2	n.a.
I	n.a.	–	1.1	–	–	0.0
Se	n.a.	4.3	8.4	–	–	17.5
Te	n.a.	1.7	–	–	–	–
Fe	n.a.	211	192	í.î.	397	255
Th	n.a.	0.17	0.02	0.14	0.12	0.09
Ga	n.a.	0.64	0.3	0.9	0.24	4.08
Sc	n.a.	108	33.7	234	276	160
Ti	n.a.	39.2	13.4	24.6	18.7	26.6
Y	n.a.	0.19	0.29	–	–	0.55
Zr	n.a.	1.84	1.16	4.91	4.8	1.97
Nb	n.a.	1.74	0.05	0.48	1.32	0.18
In	n.a.	1.48	0.03	0.35	0.6	–
Sn	n.a.	3.6	2.36	2.63	2.88	7.92
REE	n.a.	1.59	3.98	6.23	9.6	1.01
K/Rb	134	247	199	270	217	216
CO_2/CH_4	33	109	32	6	8	20

n.a., component was not analyzed; dash, component concentration is below detection limit

Table 12. (Contd.)

Component	Metamorphic		Silver–polymetallic			Silver–antimony	
	2-apk	Ark-13-190	Ark-100	A-106	Ark-107	Ark-111	Ark-112
H_2O, ppm	1945	1767	907	775	650	977	2221
Macrocomponents, g/kg water							
CO_2	10	9.26	28.34	25.36	50.81	28.26	34.80
CH_4	0.08	0.12	0.19	0.20	0.38	0.38	0.07
Cl^-	8.49	6.00	3.86	7.19	15.69	0.51	0.23
SO_4^{2-}	0.56	0.57	1.10	–	1.54	1.02	0.45
HCO_3^-	2.18	–	219.52	38.84	–	259.14	1.21
F^-	n.a.	0.57	1.10	n.a.	1.54	1.02	0.45
Na	4.91	2.00	0.82	12.86	5.21	0.45	0.15
K	0.82	0.51	0.19	1.33	0.66	n.a.	0.52
Ca	1.08	0.24	73.38	4.15	0.78	83.92	0.12
Mg	0.02	0.003	–	0.41	0.014	0.804	0.002
Microcomponents, 10^{-3} g/kg water							
Br	75	–	41.32	52	–	33.65	–
As	13	273	186	5	–	258	347
B	158	40	135	26	114	51	276
Li	1.3	0.20	3.99	540	3.18	1.22	1.83
Rb	2.1	1.65	–	5.0	8.11	–	0.65
Cs	1.8	0.65	0.63	0.5	1.94	–	–
Mo	–	0.11	3.27	0.1	0.72	1.51	0.30
Sb	28	95.39	–	48.5	19.07	–	64.32
Sr	67	13.75	–	73	53.12	121.20	–
Mn	–	4.04	–	111	62.42	180.76	–
Cu	1.7	37.45	–	62	17.00	15.84	–
Zn	202	147	–	5170	88	–	–
Cd	0.06	0.02	n.a.	19.9	0.06	–	–
Pb	0.3	–	–	36.6	0.88	1.03	–
Bi	0.03	–	–	0.1	–	0.30	–
Ba	53	6.54	30.40	60	23.86	–	–
U	–	–	0.08	–	–	–	–
W		0.18	43.36	2.2	3.52	34.68	0.15
Ag	–	0.01	–	4.0	0.03	–	–
Au	0.01	–	–	2.2	–	–	–
Co	–	0.06	2.30	1.9	0.05	3.43	–
Ni	–	1.14	1.11	465	4.69	11.33	–
V	–	–	–	4.7	–	–	–
Cr	–	0.63	11.79	6.1	1.92	11.56	–
Tl	–	1.00	0.01	0.1	0.08	0.01	0.11
Sn	0.29	–	–	6.8	0.28	–	–
Hg	–	–	0.20	1.69	0.17	0.37	–
Ge		–	0.64	n.a.	0.32	0.02	–
I	n.a.	n.a.	n.a.	0.5	n.a.	n.a.	n.a.
Se	n.a.	n.a.	n.a.	4.2	n.a.	n.a.	n.a.
Te	n.a.	n.a.	n.a.	1.3	n.a.	n.a.	n.a.
Fe	n.a.	n.a.	n.a.	297	n.a.	n.a.	n.a.
Th	n.a.	n.a.	n.a.	0.08	n.a.	n.a.	n.a.
Ga	n.a.	n.a.	n.a.	1.71	n.a.	n.a.	n.a.
Sc	n.a.	n.a.	n.a.	73.3	n.a.	n.a.	n.a.
Ti	n.a.	n.a.	n.a.	7.22	n.a.	n.a.	n.a.
Y	n.a.	n.a.	n.a.	0.02	n.a.	n.a.	n.a.
Zr	n.a.	n.a.	n.a.	0.62	n.a.	n.a.	n.a.
Nb	n.a.	n.a.	n.a.	0.33	n.a.	n.a.	n.a.
In	n.a.	n.a.	n.a.	–	n.a.	n.a.	n.a.
Sn	n.a.	n.a.	n.a.	6.78	n.a.	n.a.	n.a.
REE	n.a.	n.a.	n.a.	0.19	n.a.	n.a.	n.a.
K/Rb	398	309		263	81		803
CO_2/CH_4	137	76	153	126	135	74	522

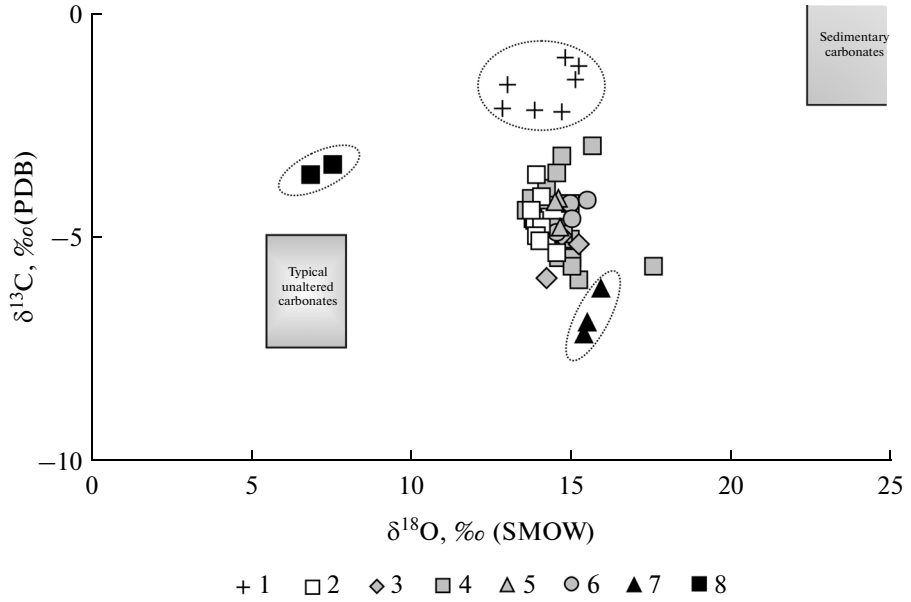

Fig. 12. Carbon and oxygen isotopic compositions of carbonates at Arkachan deposit. (1) ankerite I; (2–6) main gold stage: (2) ankerite II, (3–6) siderite: (3) ore zone 2, (4) ore zone 3, (5) ore zone 4, (6) ore zone 5; (7) siderite II; (8) calcite.

$$\Delta_{\text{siderite}-H_2O} = \delta^{18}O_{\text{siderite}} - \delta^{18}O_{H_2O} = 4.23(10^6/T^2) - 4.58(10^3/T) + 1.73, \quad (2)$$

$$\Delta_{\text{ankerite}-H_2O} = \delta^{18}O_{\text{ankerite}} - \delta^{18}O_{H_2O} = 4.12(10^6/T^2) - 4.62(10^3/T) + 1.71, \quad (3)$$

$$\Delta_{\text{calcite}-H_2O} = \delta^{18}O_{\text{calcite}} - \delta^{18}O_{H_2O} = 4.01(10^6/T^2) - 4.66(10^3/T) + 1.71. \quad (4)$$

The calculated $\delta^{18}O_{H_2O}$ of the fluid participating in the formation of early quartz–carbonate veins at 265°C are +6.9 ± 0.2‰ and +5.6 to +7.9‰ in equilibrium with quartz I and ankerite I, respectively (Fig. 13). Quartz II of the main gold stage crystallized at 350°C from the fluid, where $\delta^{18}O_{H_2O}$ varied from +7.8 to +10.5‰. The $\delta^{18}O_{H_2O}$ of the fluid that the late carbonates of this stage crystallized from are within an interval from +7.0 to +11.0‰ for siderite I (300°C) and from +6.5 to +7.2‰ for ankerite II (265°C). For a fluid coexisting with chalcedony-like quartz III and siderite II of the silver–polymetallic stage at 250°C, $\delta^{18}O$ are +5.3 to +7.9‰ and +7.4 ± 0.2‰. Cryptogranular quartz IV and calcite of silver–antimony stage crystallized from the solution enriched in light oxygen isotope ($\delta^{18}O$ = –0.5 to 0‰ and –0.6 to +0.1‰, respectively.

The oxygen isotopic composition of ore-forming fluid at the Arkachan deposit, which participated in the formation of gold mineralization (from +6.5 to +11‰) and late silver–base-metallic (from +5.3 to +7.9‰) stages, falls in the field of values ascribed to fluids of both magmatic and metamorphic origin. The $\delta^{18}O_{H_2O}$ = +5.6 to +7.9‰ obtained for the fluid, which the early preore quartz–carbonate veinlets were formed from, fall into the same interval. For both the main gold and silver–polymetallic stages, the fluids are enriched in light oxygen isotopes toward the completion of the stage. The fluid participating in the formation of the mineralization at the silver–antimony stage is characterized by $\delta^{18}O$ = –0.6 to + 0.1‰. This testifies to the involvement of heated meteoric rocks in the hydrothermal system. The obtained $\delta^{18}O_{H_2O}$ values of productive ore-forming fluids fall into the interval $\delta^{18}O_{\text{fluid}}$ from +5 to +10‰ known for gold deposits related to granitic rocks (Lang et al., 2000; McCoy et al., 1997).

The carbon isotopic composition in the fluid carbonates crystallized from is calculated from equations proposed by Ohmoto and Rye (1979) and Zhou and Dobos (1995):

$$\Delta_{\text{calcite}-CO_2} = -0.891(10^9/T^3) + 8.557(10^6/T^2) - 18.11(10^3/T) + 8.27, \quad (5)$$

$$\Delta_{\text{siderite}-CO_2} = 0.861\ (10^6/T^2) + 0.82. \quad (6)$$

Values of $\delta^{13}C$ for fluids coexisting with siderite I and ankerite II of main gold stages change from –7.8 to –4.8‰ (300°C) and from –3.9 to –2.1‰ (265°C), respectively. These values overlap an interval of –5 to –2‰, which is characteristic for CO_2 that is magmatic in origin (Kerrich, 1990). Mantle-derived car-

bon and carbon of granitic magmas are marked by $\delta^{13}C = -7$ to $-2‰$ and -6 to -2%, respectively (Jia and Kerrich, 2000). It is evident that the carbon isotopic composition of the fluids that carbonates were deposited from is close to the values accepted for these reservoirs. During the formation of the later silver–polymetallic stage, the proportion of light carbon isotope increases ($\delta^{13}C_{fl} = -9.5$ to $-8.5‰$). It cannot be ruled out that this is caused by the temperature drop of mineral formation, as according to calculations, a decrease in crystallization temperature from 300 to 250°C results in a change of $\delta^{13}C_{fl}$ by 0.5‰ and by 0.7‰ to 200°C. Another cause may be the removal of heavy carbon isotopes and thus the depletion of the residual fluid in ^{13}C caused by siderite crystallization (Zhou and Dobos, 1995). At the silver–antimony stage, calcite crystallized at ~250°C from the fluid enriched in ^{13}C ($\delta^{13}C_{fl} = -2.3$ to $-2.1‰$). Although according to Ridley and Diamond (2000), $\delta^{13}C_{fl} = -6$ to 0‰ indicates that carbon dioxide may have been supplied from mantle or released from granitic magma during its crystallization, the $\delta^{18}O_{H_2O}$, close to zero in this fluid, may indicate the probable participation of meteoric water or buried seawater during the formation of this ore. Early quartz–carbonate veinlets were formed from the fluid with $\delta^{13}C_{fl} = 0 \pm 0.6‰$, providing evidence for the derivation of carbon from host terrigenous rocks.

The sulfur isotopic composition of fluid ($\delta^{34}S_{H_2S}$) in equilibrium with sulfides at the moment of mineral formation has been calculated from equations of fractionation (Li and Liu, 2006; Ohmoto and Rye, 1979) in assumption that H_2S dominated in the solutions:

$$\Delta_{pyrite-H_2S} = \delta^{34}S_{pyrite} - \delta^{34}S_{H_2S} = 0.4\,(10^6/T^2), \quad (7)$$

$$\Delta_{chalcopyrite-H_2S} = \delta^{34}S_{chalcopyrite} - \delta^{34}S_{H_2S} = 0.05(10^6/T^2), \quad (8)$$

$$\Delta_{galena-H_2S} = \delta^{34}S_{galena} - \delta^{34}S_{H_2S} = -0.64\,(10^6/T^2), \quad (9)$$

$$\Delta_{sphalerite-H_2S} = \delta^{34}S_{sphalerite} - \delta^{34}S_{H_2S} = 0.1\,(10^6/T^2). \quad (10)$$

The $\delta^{34}S_{H_2S}$ values of fluid coexisting with early arsenopyrite I and pyrite I at 300°C vary from −7.0 to +6‰ (Fig. 14). The $\delta^{34}S_{H_2S}$ values of fluid calculated in equilibrium with late sulfides (chalcopyrite, sphalerite I, galena I) at 280°C vary from −2.0 to 14.8‰. Galena II of the silver–polymetallic stage crystallized at 250°C from fluid enriched in a light sulfur isotope ($\delta^{34}S_{H_2S} = +1.8‰$). Fluid with $\delta^{34}S_{H_2S} = -5$ to +1.6‰ participated in the formation of sulfides related to wall-rock alteration, whereas the fluid in equilibrium with sulfide of nodules in host sandstone is enriched in heavy ^{34}S ($\delta^{34}S_{H_2S} = +3.1$ to +8.1‰). Thus, most of the $\delta^{34}S$ values (60% of analyses) of the fluid forming early sulfide assemblages at the main gold stage fall within the interval of −3 to +3‰.

The sulfur isotopic compositions of the fluid participating in the formation of wall-rock sulfide disseminations and mineralization of silver–polymetallic stage fall within the same interval. This indicates that sulfur of magmatic origin participates in ore formation. At the late substage of the main gold stage, sulfur from host rocks was also involved in the hydrothermal system. The variations of sulfur isotopic composition in ore-forming fluid with depth are shown in Fig. 14. At depth, this is a narrow range (~0‰) for both early and late sulfides, which substantially widens upward.

Isotopic data on sulfide sulfur data published by Aristov et al. (2003) are close to the lower limit of variations based on our results.

$^{40}Ar/^{39}Ar$ AGE OF ORE

To estimate the time of ore formation at the Arkachan deposit, the mica has been dated using $^{40}Ar/^{39}Ar$ method of stepwise heating at the Institute of Geology and Mineralogy, Siberian Branch RAS in Novosibirsk, analyst A.V. Travin. Mica is ubiquitous in veins of the deposit, varying from individual grains to large clusters, which fill intergranular space or form spherulitic aggregates upon quartz, siderite, and early sulfides. Sporadic chalcopyrite and more frequent bismuthinite in association with native gold crystallize along cleavage of mica. Therefore, we have grounds to propose that superposition of sulfides could have disturbed K–Ar isotopic system with its rejuvenation, owing to which the $^{40}Ar/^{39}Ar$ isotopic age may correspond to the real time of the Au-bearing mineral assemblage formation.

The monofractions of light micas (muscovite, sericite) from Au-bearing quartz–siderite–sulfide veins from ore zone 2 were taken for analysis. The sampling was controlled by petrographic and geochemical methods. No indications of secondary alteration of mica have been revealed. Three samples have been analyzed; the results of measurements are given in Fig. 15. The plateau characterized by 98% of the released ^{39}Ar corresponds to $^{40}Ar/^{39}Ar$ age estimated at 101.9 ± 1.4 Ma. In the age spectrum of muscovite (two samples), the stable plateau corresponding to 76 and 81% of the released ^{39}Ar is dated at 99.6–101.1 ± 1.4 Ma. With allowance for the conservation of K–Ar isotopic system after the deposition of chalcopyrite and bismuthinite along the cleavage in micas, we suppose that the Au-bearing ore was formed approximately 100 Ma ago.

The $^{40}Ar/^{39}Ar$ isotopic age of mica from the Arkachan deposit is within the interval of $^{40}Ar/^{39}Ar$ isotopic ages (94–101 Ma) of granite and granodiorite porphyries inherent to the Endybal Complex (Layer

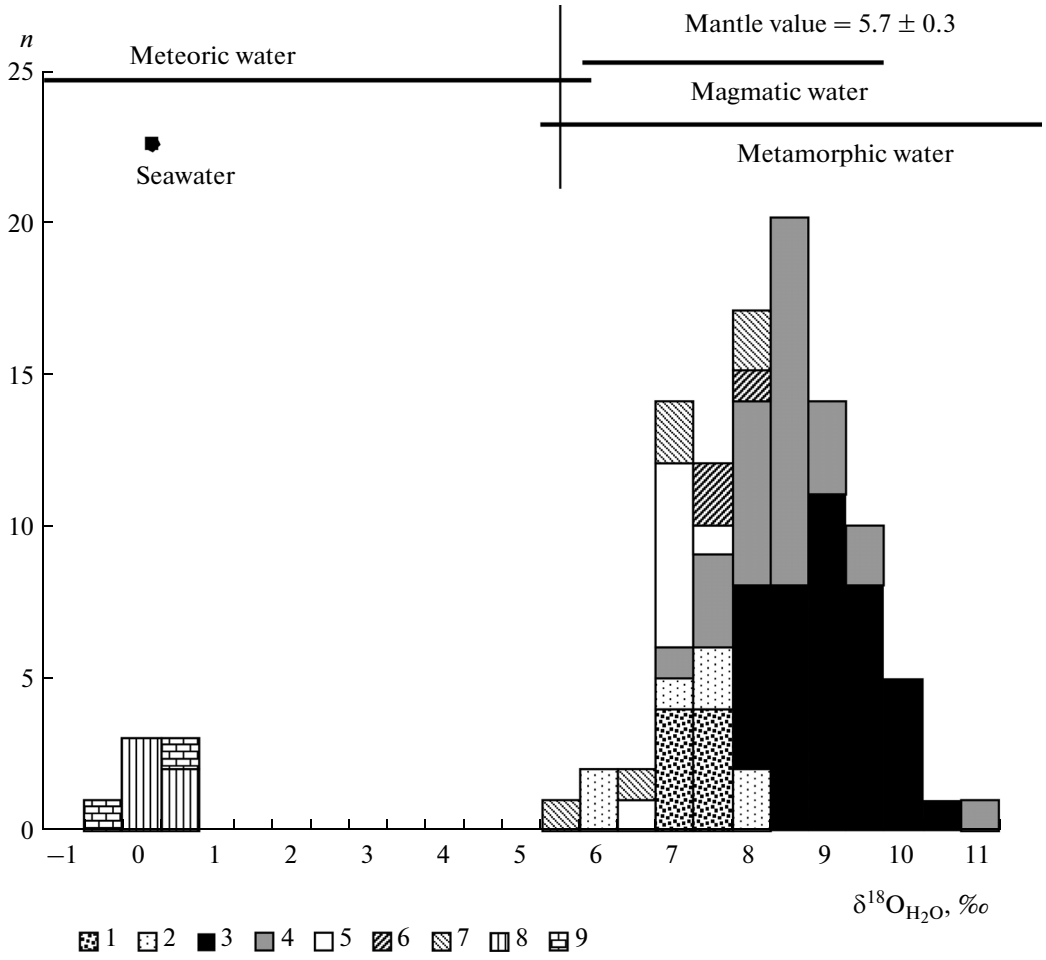

Fig. 13. Oxygen isotopic composition of hydrothermal fluid equilibrated with quartz and carbonates at Arkachan deposit. Stages: (1, 2) preore hydrothermal–metamorphic, (3–5) main gold, (6, 7) silver–polymetallic, (8, 9) silver–antimony; minerals: (1, 3, 6, 8) quartz, (2, 5, 7) ankerite, (4) siderite, (9) calcite.

et al., 2001) and Au–Bi mineralization of the Trubka occurrence (99 ± 1.2 Ma) at the Mangazeya Ag–Pb–Zn deposit situated in this district (unpublished data of G.N. Gamyanin). The above estimates are also close to the age of tin deposits associated with the transverse series of granitoids (Trunilina, 1992).

DISCUSSION

Mineralogical, isotopic-geochemical, and microthermometric study of rocks and ore at the Arkachan deposit allows us to discuss the chemistry of mineral-forming fluid in the Arkachan ore-forming system, its probable sources and evolution and to propose a genetic model of the deposit formation.

It is evident that the ore mineralogy of the Arkachan deposit is distinguished by abundant sulfides (5–70, ~10 vol %, on average), widespread siderite (10–30 vol %), and the close association of native gold with Bi minerals. The wide abundance of sulfides differs in this deposit from the low-sulfide Galechnoe, Trubka, and other Au–Bi deposits localized in this district. Carbonates are represented at orogenic gold–quartz deposits of the Upper Yana–Kolyma Mesozoides by ankerite–dolomite series and by calcite at gold–sulfide deposits, whereas siderite is predominant at the Atkachan deposit.

Hidden mineralogical and geochemical zoning is revealed at the Arkachan deposit. The Au content in pyrite and the Mg and Mn contents in carbonates increase toward the upper levels of ore zones. In contrast, quartz and arsenopyrite contents increase with depth. The temperature of mineral formation and the salinity of hydrothermal fluids rise in the same direction, and the sulfur isotopic composition of fluid becomes more homogeneous. Gold is finely dispersed in pyrite and primarily in arsenopyrite; however, its main mass occurs as fine native gold grains in close spatiotemporal association with chalcopyrite and bismuth minerals. As is known, zoning is not typical of

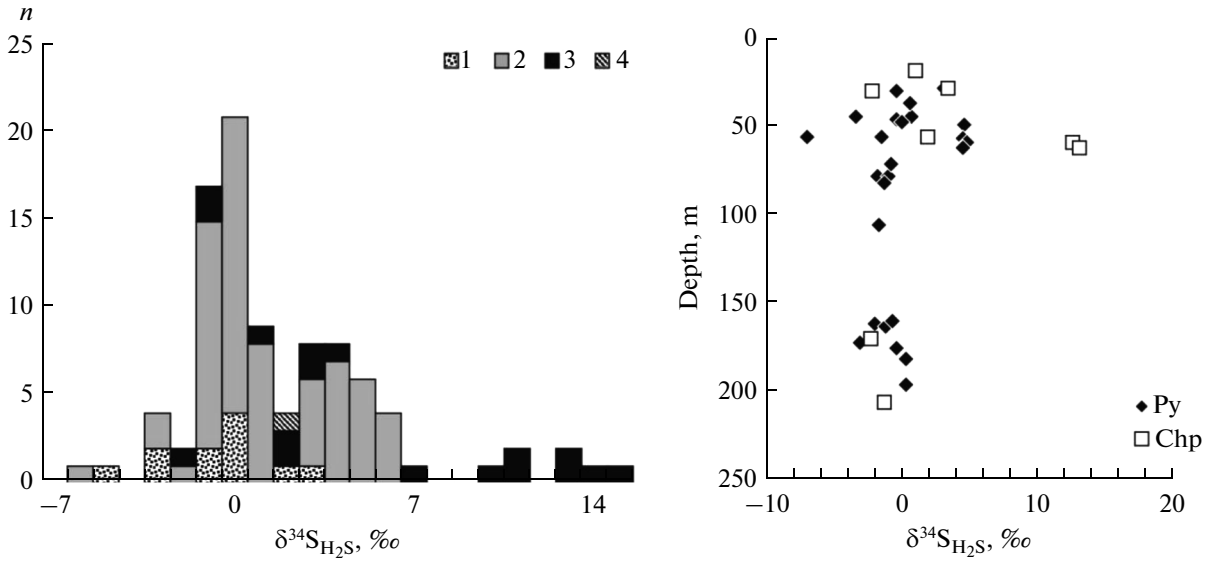

Fig. 14. (a) Sulfur isotopic composition of ore-forming fluid ($\delta^{34}S_{H_2S}$) equilibrated with sulfides at Arkachan deposit and (b) $\delta^{34}S_{H_2S}$ variations with depth. (1) sulfides from host rocks; (2) early mineral assemblages; (3) late mineral assemblages; (4) sulfides of silver–polymetallic stage. Py, pyrite, Chp, chalcopyrite.

orogenic gold deposits, but is common for intrusive-related gold deposits (Hart, 2005; Goldfarb et al., 2005). The zoning of the Arkachan deposit is apparently caused by the regular distribution of trace elements in minerals relative to the roof of granitoid pluton beneath the deposit. This pluton also controls the variation of the temperature of mineral formation.

It has been established that *the early barren quartz–carbonate veins* were formed from low-concentration (6.9–8.7 wt % NaCl equiv) aqueous salt solutions at ~265°C. The high K/Rb ratio (309–398) of these fluids and $\delta^{13}C \sim 0$ corroborate the hydrothermal–metamorphic origin of these veins.

The gold–bismuth–siderite–sulfide mineralization of the main gold stage was formed from the fluids contrasting in chemical composition: (i) a high saline (18.8–26.2 wt % NaCl equiv) $H_2O–CO_2–NaCl–MgCl_2$ solution, combined with (ii) a gaseous $CO_2–CH_4$ fluid, which coexisted in the mineral-forming system being formed as a result of phase separation of $H_2O–CO_2–CH_4–NaCl–MgCl_2$ fluid into two immiscible liquid and gaseous fluids. In addition, a moderately saline (3.7–13.4 wt % NaCl equiv) aqueous salt solution with predominant Na, Mg, and Ca chlorides occurred in the ore-forming systems. These high-temperature (279–385°C) fluids precipitated ore mineralization under moderate pressure (1.1–1.8 kbar). The late sulfides and sulfosalts released from the highly saline (19.8–22.6 wt % NaCl equiv) aqueous salt solution at a lower temperature (200–269°C). The K/Rb ratio of this fluid varies from 134 to 270, as is characteristic of granite-related fluids.

The late mineralization of *the silver–polymetallic stage* was deposited from bicarbonate–chloride Na–Ca fluids.

Thus, fluids contrasting in composition existed in the mineral-forming system of the Arkachan deposit: (i) liquid-like aqueous salt solution bearing carbon dioxide, with methane and nitrogen as admixtures; (ii) mainly carbon dioxide gaseous fluid, and (iii) aqueous salt solution. The first two are derivatives of endogenic fluid formed as products of its phase separation due to pressure release. The third aqueous salt solution may have had another origin. The latter frequently occurs together with aqueous salt solutions bearing carbon dioxide in ore-forming systems (Bortnikov, 2006) and probably is heated meteoric water.

The fluid responsible for deposition of gold–bismuth–siderite–sulfide mineralization at the Arkachan deposit differs in chemical composition from the ore-forming fluids at orogenic gold deposits. The latter, as a rule, are formed from liquid $H_2O–CO_2 \pm CH_4 \pm N_2–NaCl$ fluid low- to moderate-concentrated with salinity of 3–12 wt % NaCl equiv coexisting with gaseous $CO_2 \pm CH_4$ fluid (Goldfarb et al., 2005; Bortnikov, 2006). Aqueous salt solutions with high salinity also take part in ore formation (Bortnikov, 2006). Their origin is a matter of debate. They are suggested to be metamorphic ore (Goldfarb et al., 2005) and are linked to magmatic activity and thermal transformation of rocks in the supraintrusive zone (Bortnikov et al., 2007). The ore at the intrusion-related gold deposits was formed from high-saline $H_2O–CO_2–NaCl$ fluids (≥30 wt % NaCl equiv) and low-salinity

(≤5 wt % NaCl equiv) gaseous fluids consisting primarily of CO_2, which arose as a result of phase separation. Moderately saline (≤10 wt % NaCl equiv) fluids have been revealed at certain deposits pertaining to this type. Fluids with a higher salinity (4–40 wt % NaCl equiv) participated in mineral formation at later stages. It is suggested that these fluids, contrasting in chemistry, were formed as a result of different behavior of volatile components (water, carbon dioxide, chlorine) being released from felsic magmas crystallizing at different depths (Baker, 2002). Chemical composition of mineral-forming $H_2O–CO_2 \pm CH_4 \pm N_2–NaCl \pm CaCl_2$ fluids that the ore of the Arakchan deposit was formed from are in many aspects similar to the fluids that created Ag–Pb–Zn carbonate orebodies at the Mangazeya, Prognoz, and Kupol'noe deposits in the Verkhoyansky district (Klubnikin et al., 2011; Gamyanin et al., 1998, 2001). A magmatic origin connected with evolution of Sn-bearing hydrothermal–magmatic systems was suggested for these fluids. The later saline aqueous solution was involved in both systems as well.

Thus, the chemistry of the fluid parental to the Arkachan deposit allows us to assume its link to granitic magmatism by analogy with gold- and silver-bearing systems. Methane and nitrogen may have been supplied therein as products of reactions with host rocks.

The oxygen, carbon, and sulfur isotopic compositions of this fluid indicate that magmatic components are predominant. At the same time, the $\delta^{18}O_{H_2O}$ value does not rule out the involvement of metamorphic water, which was formed as a product of dehydration of minerals in the heated supradomal zone of intrusion. The heated meteoric water enriched in ^{16}O was involved in the system at the late stage of its evolution. The carbon isotope ratios do not allow us to determine the source of carbon unequivocally. Carbon dioxide with calculated $\delta^{13}C$ may have been supplied from the mantle or released from granitic magma during its crystallization. The $\delta^{34}S$ (0 ± 3‰) also may indicate involvement of mantle-derived sulfur or that released from granitic magma containing a mantle component. At the same time, substantial variations of $\delta^{34}S$ (up to 16‰) can be explained by sulfur supply from various sources rather than by variations of temperature, pH, or redox conditions of mineral formation. Hydrogen sulfide enriched in ^{34}S was recovered from sulfides of country rocks (seawater sulfur), whereas H_2S with negative $\delta^{34}S_{H_2S}$ was released from granitic magma assimilating sedimentary rocks (Ohmoto, 1986). C, O, and S isotopic compositions suggest predomination of magmatic fluid participating in the formation of gold mineralization, while a value of $CO_2/CH_4 = 6.5–110$ indicates elevated methane concentrations therein.

The mineralization of the silver–antimony stage was formed from a fluid significantly differing in isotopic

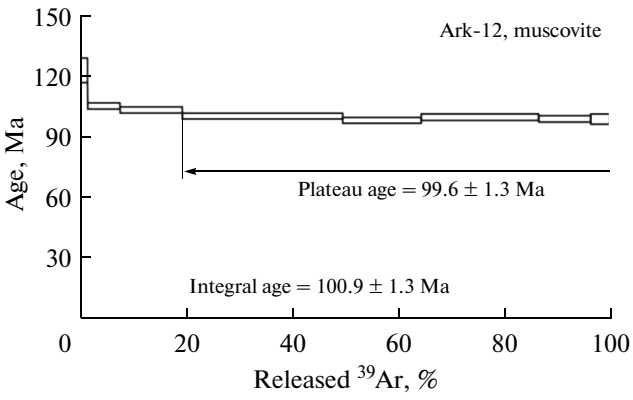

Fig. 15. Ar/Ar age of mica from productive veins at Arkachan deposit.

parameters from fluids of the Arkachan hydrothermal system described above. Values of $\delta^{18}O_{H_2O}$ (–0.6 to +0.1‰) inherent to this fluid assume the participation of meteoric or buried seawater in ore formation. In addition, the role of CO_2 (CO_2/CH_4 up to 522) increases in these solutions along with increases in K/Rb ratio up to 803.

The REE patterns of rocks, minerals (carbonates, quartz), and fluid inclusions in quartz from the Arkachan deposit display increase in REE contents in rocks affected by hydrothermal alteration, occurrence of negative Eu anomaly, and correlation of total REE contents with Cl, B, Rb, and Cs concentrations in fluids. Eu-deficient fluids can be derivatives of granitic plutons. The negative Eu anomaly has been detected not only in minerals and fluid inclusions, but also in hydrothermally altered rocks supporting significant role of magmatic hydrothermal solutions in ore formation. Decreased total REE concentrations correspond to increases in f_{O_2} and to depletion of fluid in salts. The lower REE concentrations in fluid inclusions as compared with known data on magmatic fluids (Banks et al., 1994) suggest that the fluids separated from a hypabyssal (~3 km) magma chamber (Lukanin and Dernov-Pegaev, 2008). Ore zone 2 is more deeply eroded and represents a deeper level of mineralization. The lower REE contents in carbonates from this ore zone as compared with other zones are probably explained by the low concentration of REE in magmatic fluid.

Thus, mineralogical and geochemical study of the Arkachan deposit has shown that this deposit differs from orogenic gold deposits in its mineralogy, distribution of trace elements in minerals, and composition of mineral-forming fluid; it has some features similar to those of gold and silver deposits genetically related (but not identical) to granitic magmatism. Therefore, it is reasonable to regard the Arkachan deposit as a new

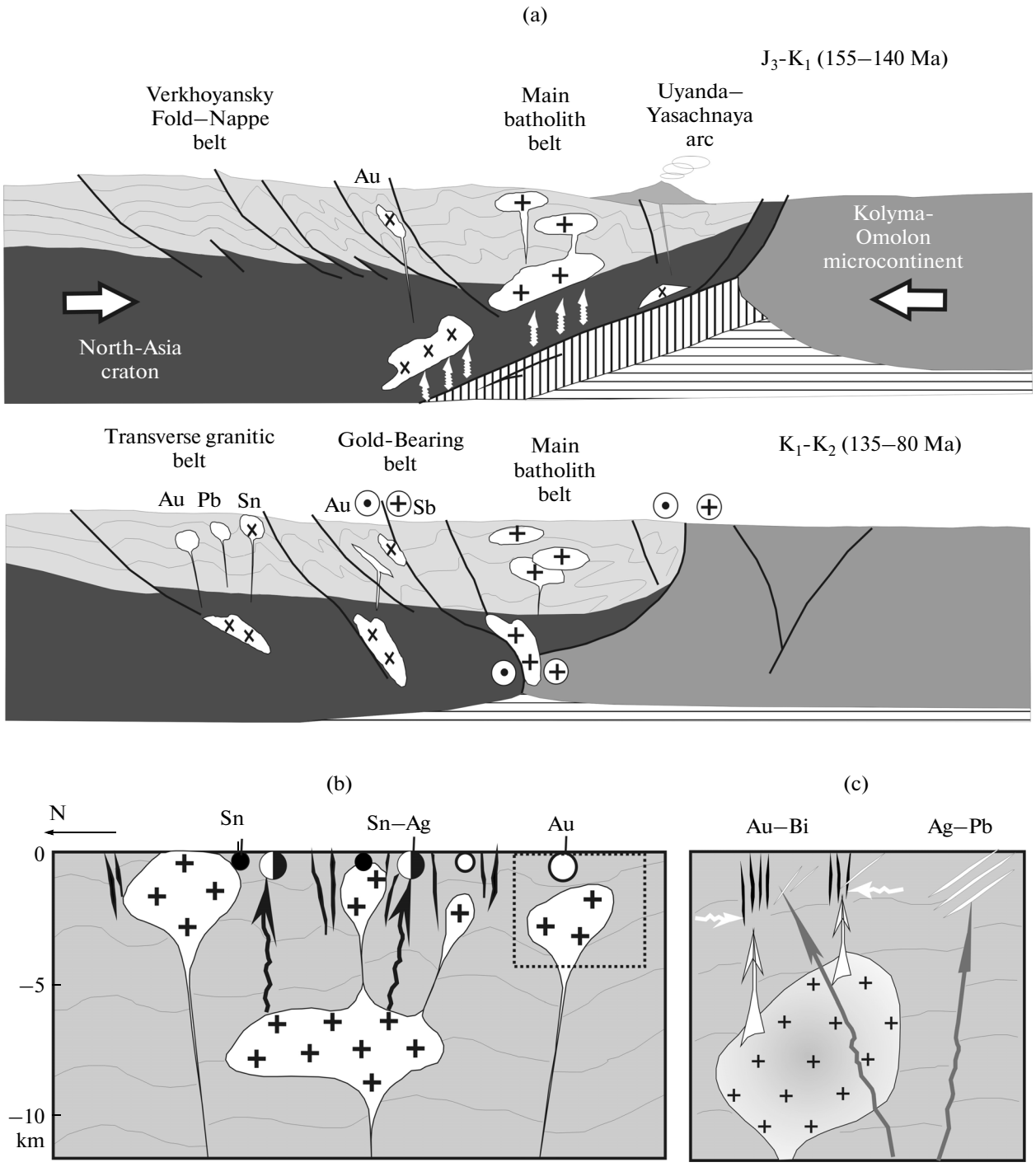

Fig. 16. (a) Schematic cross-section of Tin metallogenic zone, (b) geological and genetic model of Arkachan ore-forming system. Mineralization: Sn, cassiterite–silicate; Sn–Ag, cassiterite–sulfide; Au, gold–polysulfide; Au–Bi and Ag–Pb, productive gold–bismuth–siderite–polysulfide and silver–polymetallic mineralization in close-up (c).

gold–bismuth–siderite–sulfide type that is derivative from tin-bearing ore–magmatic systems.

What are the conditions of the origin and evolution of the ore-magmatic systems that generate Arkachan-type deposits?

It is thought that the formation of the Arkachan deposit bearing the features of both gold–bismuth and cassiterite–sulfide mineralization is determined by the moderate depth of its transitional magma chamber as indicated by geochemical specialization of granitic

rocks of the Upper Yana–Kolyma Mesozoides for Au and Sn to the same extent (Gamyanin et al., 1999). In contrast to the hypabyssal level (1.5–2.0 km) of magma chambers producing cassiterite–silicate and gold–bismuth mineralization and to abyssal (>8 km) chambers producing cassiterite–sulfide deposits, medium-seated magma chambers do not create the conditions for specialization of ore-bearing fluid for gold or tin.

Let us consider the geodynamic conditions of deposit formation. The North Tirekhtyakh Fault Zone, which controls localization of tin–silver–polymetallic and gold (Arkachan) mineralization of transverse series of the West Verkhoyansky Province, originated in the Early Cretaceous, when the frontal collision of the Kolyma–Omolon microcontinent with the North Asian Craton changed its direction to movement at an oblique angle. This period was characterized by the arising of transverse faults and emplacement of transverse belts of granitic plutons. These zones extend for more than 300 km at a width of 30 km. According to geophysical data, they are traced to a depth of 20 km. The ages of igneous rocks and related ore deposits become younger along the strike of transverse series from 132 Ma at the northeastern end (Derbeke–Nel'gekhe pluton) to 100 Ma at the southwestern end (Endybal stock and the stock beneath the Arkachan deposit inferred from geophysical data). The Ar/Ar age of orebodies at the Arkachan deposit is estimated at 99.6 to 101.9 ± 1.4 Ma by the dating of muscovite from ore veins. The depth of magma generation in transverse series (28–30 km) causes elevated basicity and lower viscosity of melts, as well as the enrichment of related deposits in sulfides. The decrease in the force of magma squeezing in transverse fault zones toward the Siberian Platform led to increase in depth of magma chambers. The genetic model of the Arkachan deposit (Fig. 16) is based on the thermobarogeochemical, isotopic geochemical, and geochronological data.

At the final stage of the collision (100–105 Ma), a magma chamber arose at a depth of 4–5 km from the paleosurface at intersection of the North Tirekhtyakh and the Kygyltas fault zones. This chamber generated an ore-bearing bicarbonate–Na-chloride fluid saturated with Li, B, As, Zn, Fe, Mn, and Cu. The ore was formed at a depth of 3.0–2.5 km from the paleosurface at 385–250°C with the participation of solutions whose concentrations correspond to 26–19 wt % NaCl equiv. Strike-slip offsets along large NW-trending faults of the Verkhoyansky Fold Region, including the Kygyltas Fault, were related to the reactivation of the Uda–Murgal volcanic arc 90–80 Ma ago. Ore-bearing fluids enriched in silver and retaining the geochemical characteristics of Sn-bearing ore–magmatic system was supplied along these faults.

ACKNOWLEDGMENTS

We thank N.V. Christoforova, L.M. Popova, S.A. Gorbacheva, A.S. Avdeenko, Yu.V. Vasyuta, S.G. Kryazhev, L.N. Berdnikov, and A.V. Travin for carrying out analytical procedures. The study was supported by the Presidium of the Russian Academy of Sciences (Program of Fundamental Research no. 5), the Russian Scientific Foundation (project no. 14-17-00465), and the Division of Earth Sciences, Russian Academy of Sciences (Program no. 2).

REFERENCES

Anikina, E.Yu., Gamyanin, G.N., and Bortnikov, N.S., Sulfur isotopic composition of sulfides at the Mangazeya silver deposit, eastern Sakha-Yakutia, Russia, *Geol. Ore Deposits*, 2010, vol. 52, no. 6, pp. 438–458.

Aristov, V.V., Konstantinov, M.M., Orlova, G.Yu., et al., Arkachan gold deposit, western Verkhoyansk area, *Rudy Met.*, 2003, no. 4, pp. 15–30.

Baker, T., Emplacement depth and carbon dioxide-rich fluid inclusions in intrusion-related gold deposits, *Econ. Geol.*, 2002, vol. 97, pp. 1111–1117.

Banks, D.A., Yardley, B.W.D., Campbell, A.R., and Jarvis, K.E., REE composition of an aqueous magmatic fluid: a fluid inclusion study from the Capitan Pluton, New Mexico, USA, *Chem. Geol.*, 1994, vol. 113, pp. 259–272.

Bau, M. and Möller, P., Rare earth elements fractionation in metamorphogenic hydrothermal calcite, magnesite and siderite, *Mineral. Petrol.*, 1992, vol. 45, p. 231.

Blevin, P.L. and Chappel, B.W., Chemistry, origin, and evolution of mineralized granites in the Lachlan fold belt, Australia: the metallogeny of I- and S-type granites, *Econ. Geol.*, 1995, vol. 90, pp. 1604–1619.

Bodnar, R.J. and Vityk, M.O., Interpretation of microtermometric data for H2O–NaCl fluid inclusions, *Fluid inclusions in minerals: methods and applications*, Pontignano: Siena 1994, pp. 117–130.

Borisenko, A.S., Cryometric study of salt composition of gas–liquid inclusions in minerals, *Geol. Geofiz.*, 1977, no. 8, pp. 16–27.

Bortnikov, N.S., Gamyanin, G.N., Vikent'eva, O.V., and Prokof'ev, V.Yu., The Arkachan world-class intrusion-related gold deposit, eastern Yakutia, Russia: REE, fluid inclusion and stable isotope studies, *Let's Talk Ore Deposits. Proceedings of the 11th Biennial Meeting SGA 2011, Antofagasta (Chile)*, 2011, pp. 580–582.

Bortnikov, N.S., Gamyanin, G.N., Alpatov, V.V., et al., Mineralogy, geochemistry and origin of the Nezhdaninsk gold deposit (Sakha-Yakutia, Russia), *Geol. Ore Deposits*, 1998, vol. 40, no. 2, pp, 121–138.

Bortnikov, N.S., Geochemistry and origin of the ore-forming fluids in hydrothermal–magmatic systems in tectonically active zones, *Geol. Ore Deposits*, 2006, vol. 48, no. 1, pp. 1–22.

Bortnikov, N.S., Gamyanin, G.N., Vikent'eva, O.V., et al., Fluid composition and origin in the hydrothermal system of the Nezhdaninsky gold deposit, Sakha (Yakutia), Russia, *Geol. Ore Deposits*, 2007, vol. 49, no. 2, pp. 87–128.

Brown, P., FLINCOR: a computer program for the reduction and investigation of fluid inclusion data, *Am. Mineral.*, 1989, vol. 74, pp. 1390–1393.

Chappell, B.W. and White, A.J.R., Two contrasting granitic types: 25 years later, *Austral. J. Earth Sci.*, 2001, vol. 48, no. 4, pp. 489–500.

Gamyanin, G.N., Anikina, E.Yu., Bortnikov, N.S., et al., The Prognoz silver–polymetallic deposit, Sakha: mineralogy, geochemistry, and origin, *Geol. Ore Deposits*, 1998, no. 5, pp. 391–407.

Gamyanin, G.N., Bakharev, A.G., Goryachev, N.A., and Alpatov, V.V., *Mezozoiskaya metallogeniya zolota i serebra severo-vostoka Azii, Geologiya I tektonika platformennykh i orogennykh oblastei severo-vostochnoi Azii* (Mesozoic Metallogeny of Gold and Silver of Northeastern Asia. Geology and Tectonics of the Platform and Orogenic Areas of Asia) Yakutsk: YaNTs, 1999.

Gamyanin, G.N., Bortnikov, N.S., Alpatov, V.V., et al., The Kupol'noe silver–tin deposit (Sakha Republic, Russia): an example of the evolution of an ore-magmatic system, *Geol. Ore Deposits*, 2001, vol. 43, no. 6, pp. 442–467.

Gamyanin, G.N., *Mineralogo-geneticheskie aspekty zolotogo orudeneniya Verkhoyano-Kolymskikh mezozoid* (Mineralogical–Genetic Aspects of Gold Mineralization in the Verkhoyansk–Kolyma Mesozoides), Moscow: "GEOS", 2001.

Goldfarb, R.J., Baker, N., and Dubé, B., Distribution, character and genesis of gold deposits in metamorphic terranes, *Econ. Geol.,* 2005, vol. 100, pp. 407–450.

Gutorovich, D.I. and Izarov, V.T., *Report on Aeromagnetic Works On A Scale 1 : 50000 Conducted in the Chochimbal District In 1965*, Nyurba, 1966.

Hart, C.J.R., Classifying, distinguishing and exploring for intrusion-related gold systems, *The Gangue: Geological Association of Canada, Mineral Deposits Division Newsletter*, 2005, vol. 87, pp. 1–9.

Irber, W., The lantanide tetrad effect and its correlation with K/Rb, Eu/Eu*, Sr/Eu, Y/Ho, and Zr/Hf of evolving peraluminous granite suites, *Geochim. Cosmochim. Acta*, 1999, vol. 63, nos. 3–4, pp. 489–508.

Ivensen, Yu.P., Amuzinskii, V.A., and Nevoisa, G.G., *Stroenie, istoriya razvitiya, magmatizm i metallogeniya severnoi chasti Verkhoyanskoi skladchatoi zony* (Structure, Evolution, Magmatism, and Metallogeny of the Northern Verkhoyansk Fold Zone), Novosibirsk: Nauka, 1975.

Jia, Y. and Kerrich, R., Giant quartz vein systems in accretionary orogenic belts: the evidence for a metamorphic fluid origin from $\delta^{15}N$ and $\delta^{13}C$ studies, *Earth Planet. Sci. Lett.,* 2000, vol. 184, pp. 211–224.

Kalyuzhnyi, V.A., *Osnovy ucheniya o mineraloobrazuyushchikh flyuidakh* (Principles of Theory on Mineral-Forming Fluids), Kiev: Nauk. dumka, 1982.

Kerrich, R., Mesothermal gold deposits: a critique of genetic hypotheses, *Proceedings of Nuna Conference on Greenstone Gold and Crustal Evolution*, Timmins: Geol. Assoc. Canada, 1990, pp. 13–31.

Klubnikin, G.K., Prokof'ev, V.Yu., Anikina, E.Yu., and Bortnikov, N.S., Contrast fluids in the mineral-forming system of the Mangazeiskoe silver deposit (Republic Sakha (Yakutia)), *Dokl. Earth Sci.*, 2011, vol. 438, no. 2, pp. 779–781.

Konstantinov, M.M., Bystrova, A.K., and Fridovsky, V.Yu. Stratigraphic level of localization of the gold and silver deposits in the Verkhoyansk and Central Kolyma metallogenic provinces, *Tikhookean. Geol.*, 2002, vol. 21, no. 6, pp. 105–111.

Kostin, A.V., Zoning of the Arkachan gold–copper deposit, Western Verkhoyansk area, *Otechestvennaya Geol.*, 2003, no. 6, pp. 24–29.

Kryazhev, S.G., Prokof'ev, V.Yu., and Vasyuta, Yu.V., Application of ICP-MS for analysis of ore-forming fluids, *Vestn. Mosk. Gos. Univ. Ser. 4: Geol.*, 2006, no. 4, pp. 30–36.

Lang, J.R., Baker, T., Hart, C.J.R., and Mortensen, J.K., An exploration model for intrusion-related gold systems, *Soc. Econ. Geol. Newslett.,* 2000, vol. 40.

Lang, J.R. and Baker, T., Intrusion-related gold systems: the present level of understanding, *Miner. Deposita*, 2001, vol. 36, pp. 477–489.

Layer, P.W., Newberry, R., Fujita, K., et al., Tectonic setting of the plutonic belts of Yakutia, northeast Russia, based on $^{40}Ar/^{39}Ar$ and trace element geochemistry, *Geology*, 2001, vol. 29, pp. 167–170.

Lehmann, B., *Metallogeny of tin. Lecture Notes in Earth Sciences*, Berlin: Springer-Verlag, 1990.

Li, Y.B. and Liu, J.M., Calculation of sulfur isotope fractionation in sulfides, *Geochim. Cosmochim. Acta*, 2006, vol. 70, pp. 1789–1795.

Lüders, V., Moller, P., and Dulskl, P., REE fractionation in carbonates and fluorite, *Monogr. Ser. Mineral Dep.,* 1993, vol. 30, pp. 133–150.

Lukanin, O.A. and Dernov-Pegarev, V.F., REE in magmatic fluids formed during ascent of granitic melts to the Earth's surface, "Electron. Sci. Inform. Journal—Vestn. Otd. Nauk Zemle Ross. Akad. Nauk, 2008, vo. 1(26). http://www.scgis.ru/russian/cp1251/h_dgggms/1-2008/informbul-1_2008/magm-21e.pdf

McCoy, D., Newberry, R.J., Layer, P.W., et al., Plutonic-related gold deposits of interior Alaska, *Econ. Geol. Monogr.*, 1997, vol. 9, pp. 191–241.

Mozgova, N.N., *Nestekhiometriya i gomologicheskie ryady sul'fosolei* (Non-stoichiometry and homological series of sulfosalts), Moscow: Nedra, 1985.

Ohmoto, H. and Rye, R.O., Isotope of sulfur and carbon, in *Geochemistry of Hydrothermal Ore Deposits*, New York: Wiley and Sons, 1979, pp. 509–567.

Ohmoto, H., Stable isotope geochemistry of ore deposits, *Rev. Mineral.*, 1986, vol. 16, p. 491–560.

Parfenov, L.M., Vetluzhskikh, V.G., Gamyanin, G.N., et al., Main metallogenic units of the Sakha Republic (Yakutia), Russia, *Int. Geol. Rev.*, 1999, vol. 41, no. 5, pp. 425–457.

Prokof'ev, V.Yu. and Naumov, V.B., Geochemical features of ore-forming solutions of the Zyryanovo sulfide–polymetallic deposit (Rudnyi Altai), *Geokhimiya*, 1987, no. 3, pp. 375–386.

Prokof'ev, V. Yu and Pek, A. A. Problems in estimation of the formation of hydrothermal deposits by data on pressure of mineralizing fluid, *Geol. Ore Deposits,* 2015, vol. 57, no. 1, pp. 1–20.

Roedder, E., *Fluid Inclusions*, Washington: Mineral Soc. Am., 1984.

Ridley, J.R. and Diamond, L.W., Fluid chemistry of orogenic lode gold deposits and implications for genetic models, *Gold in 2000, Seg. Rew.*, 2000, vol. 13, pp. 141–162.

Sillitoe, R.H., Giant and bonanza gold deposits in the epithermal environment: assessment of potential genetic factors, *Soc. Econ. Geol. Sp. Publ.*, 1993, vol. 2, pp. 125–156.

Taylor, S.R. and McLennan, S.M., *The Continental Crust: its Composition and Evolution* Oxford: Blackwell, 1985.

Thompson, J.F.H., Sillitoe, R.H., Baker, T.J.R., and Mortensen, J.K., Intrusion-related gold deposits associated with tungsten-tin provinces, *Mineral. Deposita*, 1999, vol. 34, pp. 323–334.

Topa, D. and Makovicky, E., The crystal chemistry of cosalite based on new electron-microprobe data and single-crystal determinations of the structure, *Can. Mineral.*, 2010, vol. 48, pp. 1081–1107.

Trunilina, V.A., *Geologiya i rudonosnost' pozdnemezozoiskikh magmaticheskikh obrazovanii severo-vostoka Yakutii* (Geology and Ore Potential of the Late Mesozoic Magmatic Complexes of Northeastern Yakutia), Novosibirsk: Nauka, 1992.

Vikent'eva, O.V., Gamyanin, G.N., and Bortnikov, N.S., REE in quartz fluid inclusions from gold deposits from north-east of russia, *Central Eur. J. Geosci.*, 2012, vol. 4, no. 2, pp. 310–323.

Zadorozhnyi, D.N., Tectonophycail criteria for predicting mineralization of the Verkhoyansk silver-bearing province, *Extended Abstract of Cand. Sci. (Geol.-Min.) Dissertation*, Moscow, 2002.

Zhang, L.-G., Liu, J.-X., Zhou, H.B., and Chen, Z.-S., Oxygen isotope fractionation in the quartz–water–salt system, *Econ. Geol.*, 1989, vol. 89, pp. 1643–1650.

Zheng, Y.F., Oxygen isotope fractionation in carbonate and sulfate minerals, *Geochem. J.*, 1999, vol. 33, pp. 109–126.

Zhou, T. and Dobos, S.K., A carbon and oxygen stable isotopic study of the siderite alteration in the Black Ridge gold deposit, Clermont, Central Queensland, *Mineral. Deposita*, 1995, vol. 30, no. 1, pp. 20–29.

Translated by V. Popov